Mechanistic Aspects and Side Reactions during Reversible Mg Deposition and Oxygen Reduction on a Pt Film Electrode in BMP-TFSI-Based Electrolytes: A DEMS Study

Zenonas Jusys[a] and R. Jürgen Behm*[a, b]

Reversible Mg deposition/stripping and O_2 reduction/evolution on a Pt film electrode in neat and O_2-saturated 1-butyl-1-methylpyrrolidinium bis(trifluoromethylsulfonyl) imide (BMP-TFSI) electrolytes, containing $Mg(TFSI)_2$ and/or $Mg(BH_4)_2$ as Mg source as well as $Mg(BH_4)_2$ and/or the crown ether 18-c-6 as additive, were investigated by online differential electrochemical mass spectrometry (DEMS) and by scanning electron microscopy/energy dispersed X-ray spectroscopy. Combined cyclic voltammetry and DEMS measurements reveal a complex network of partial reactions, including borohydride electrooxidation by reaction with water or O_2, chemical bulk reaction of these components, as well as electro-oxidation of H_2, and electrolyte decomposition, in addition to the primary reactions

Mg deposition/stripping and ORR/OER. They provide detailed insights into the potential dependent reactions occurring under these conditions, demonstrating that also the additive 18-c-6 undergoes decomposition upon reduction of Mg^{2+}. Contributions from chemical bulk reactions are resolved by DEMS measurements in borohydride containing solution without a Pt electrode. Electrocatalytic borohydride oxidation, explored by similar measurements with a Pt electrode, can lead to H_2 or H^+ formation. Under open circuit potential conditions, charge compensation by the ORR results in the formation of a mixed potential. Consequences of these findings for applications in Mg-air batteries are discussed.

Introduction

Multivalent metal-ion and metal-air batteries have a high potential to fulfill the demands for an improved energy density and safe operation.[1] Among the various fundamental problems to be resolved, this requires a molecular-level understanding of the solvation/complexation of the multivalent metal ions, as a basis for a rational design and development of stable electrolytes for these next-generation post-Li batteries.[2,3] In spite of their larger charge density the multivalent metal ions are, however, likely to exhibit a higher tendency for ion pairing or ion clustering, which in turn leads to a lower ion mobility.[2,4] Furthermore, they may also enhance the tendency for electrolyte decomposition and thus reduce the stability of the electrolyte, resulting in the formation of a non-conductive, passivating layer at the electrode surface.[2,3] Third, so far there are only a limited number of affordable intercalation materials.[5,6] Especially the divalent metal Mg has attracted considerable attention recently due to the high natural abundance of Mg, its

low cost, and its high theoretical capacity, as well as a low redox potential (reasonably high cell voltage), but also in this case the successful formulation of suitable stable organic electrolytes was found to be highly challenging.[2,3,5,7–9]

Recently we started a systematic study on the deposition/stripping of Mg and the reduction/evolution of O_2 from/in a room temperature ionic liquid (RTIL), specifically in 1-butyl-1-methylpyrrolidinium bis(trifluoromethylsulfonyl) imide (BMP-TFSI),[10–15] which will be continued in the present study. RTILs are attractive candidates as solvent in Li and post-Li ion batteries because of their wide electrochemical stability window, low flammability and low vapor pressure,[16–18] where the latter is especially important for metal-air batteries.[19–24] However, they also show some disadvantages such as the above-mentioned reduced mobility due to ion pair formation,[25] which is more pronounced for more highly charged metal ions. Furthermore, the stability of these RTILs can be affected by the presence of the metal ions, due to complex formation with the metal ions. This may create a severe obstacle in the RTIL environment due to the high concentration of counter ions. Indeed, reductive decomposition of the TFSI⁻ anion in the presence of Mg had been identified in several studies and proposed as a major reason for the observed passivation of the electrode for reversible Mg deposition/stripping or O_2 reduction/evolution.[10,11,15,25–27] This was attributed to Mg^{2+} complex formation, where TFSI anions are coordinated to Mg^{2+},[28,29] and decomposition of TFSI⁻ upon reduction of the Mg^{2+} central ion to Mg^+. Another problem can arise from trace impurities of water in the RTIL, which lead to the formation of stable oxidic passivation layers.[30] To avoid such effects, additives are added to the RTIL such as BH_4^-,[16,31,32] or the borane dimethylamine

[a] Dr. Z. Jusys, Prof. Dr. R. J. Behm
Institute of Theoretical Chemistry, Ulm University,
Oberberghof 7, 89081 Ulm, Germany
E-mail: juergen.behm@uni-ulm.de

[b] Prof. Dr. R. J. Behm
Helmholtz Institute Ulm Electrochemical Energy Storage (HIU),
Helmholtzstr. 11, 89081 Ulm, Germany

complex NBH,[14] Figure 4 which may act as water scavenger, and/or complexing agents such as glymes,[29] ethers,[15,27,33] or also BH_4^-,[17,34,35] which should reduce or even exclude direct interaction between Mg and the RTIL components. Under model conditions, reversible Mg deposition/stripping was shown to be possible in the presence of both BH_4^-, introduced as $Mg(BH_4)_2$, and the 18-c-6 crown ether as a complexing agent.[15] Alternatively, the RTIL anion can be modified to exclude Mg-induced decomposition, for example, by alkoxy-functionalization, such that the functionalized anion can displace the $TFSI^-$ group from the coordination sphere of Mg^{2+}.[36] This allowed reversible Mg deposition/dissolution with high coulombic efficiency, and it was suggested that the coordination sphere of the transient Mg^+ ions may play a key role in reversible Mg deposition/dissolution. In a combined experimental and theoretical study we could recently show that the crown ether 18-crown-6 (18-c-6) indeed binds more strongly to Mg than the $TFSI^-$ anion and can therefore displace TFSI from the inner coordination sphere of the Mg^{2+} cations at room temperature.[15] On the other hand, the bond is not too strong, such that Mg deposition is still possible.[15] This led to the conclusion that the optimum additive should have an interaction energy with the central metal ion that is neither too weak, to facilitate displacement of the TFSI anion in this case, nor too strong, to still allow Mg deposition or formation of re-oxidizable Mg oxy-species, along the lines predicted by the Sabatier principle.[37,38] Finally it should be noted that a recent study showed that in contrast to the positive effect of 18-c-6 on reversible Mg deposition/stripping the closely related crown ether 15-c-5 actually led to an inhibition of that reaction, which was attributed to a too strong complexation of the Mg^{2+} ion.[39]

In this work we present and discuss results of a systematic online differential electrochemical mass spectrometry (DEMS) study on the reversible Mg deposition/stripping (in O_2-free electrolytes) and O_2 reduction (ORR)/evolution (OER) (in O_2-saturated electrolyte) on a Pt film electrode during potential cycling in four different BMP-TFSI based electrolytes of different composition, containing different concentrations of Mg^{2+} (as $Mg(TFSI)_2$ and $Mg(BH_4)_2$), of BH_4^- (as $Mg(BH_4)_2$) and of the crown ether 18-c-6 (see Table 1). This mainly differs from our previous studies[10–15] either by the different additive used as water scavenger, with BH_4^- in the present case and NBH in Ref. [14], or by the enforced presence of O_2 in the electrolyte, which was not the case in Ref. [15]. Also, different from the purely electrochemical measurements mainly used in our previous studies,[10,11,15] DEMS measurements provide access to the potential dependent formation of gaseous products of the main reactions or of possible side reactions. Furthermore, the present measurements were performed at a fifty times slower potential

scan rate than in our previous work with purely electrochemical detection, to be closer to realistic situations in most battery applications, especially those anticipated for Mg-air batteries, where the potential variation during discharge is rather slow. The much slower potential variation may affect the overall performance in a number of different ways. On the one hand, it should reduce mass transport limitations and the Ohmic losses caused by the rather low Mg^{2+} concentrations, which result from the low solubility of the chemicals in the BMP-TFSI solvent, by the high viscosity and by the poor electrical conductivity of the latter. On the other hand, it may affect the impact of trace impurities such as residual water or oxygen because of the longer times available for the uptake of poisons. Both of these impurities were shown to severely affect and even inhibit Mg deposition and stripping.[40–42]

We start with characterizing Mg deposition/stripping and gas evolution in the O_2-free electrolytes. We mainly present these DEMS data as temporal profiles of the potential, of the Faradaic current and of different mass spectrometric traces, as they allow a better identification of correlations between the different features. For better comparison with previous electrochemical studies, however, we also present conventional CVs and briefly summarize their main features in the Supporting Information (SI). The resulting electrodeposits were characterized by scanning electron microscopy (SEM) and energy dispersive X-ray spectroscopy (EDS). Results on the gas evolution in a borohydride containing electrolyte under purely chemical conditions, without a Pt electrode, both in the presence and absence of O_2, and the gas evolution/consumption upon interaction of the different BMP-TFSI based electrolytes with a Pt film electrode under open-circuit conditions, also in the presence and absence of O_2 are presented in the next section. Finally, these latter measurements were continued under potential control, monitoring the Faradaic current and the different mass signals during 3 complete cycles in the following section. With these latter measurements, which allow us to discriminate between electrocatalytic reactions and chemical bulk reactions, we aim at a better understanding of the role of the borohydride additive in the reversible Mg deposition/stripping reaction and ORR/OER. For similar reasons as above, we also in this case present conventional CVs and briefly summarize their main features in the SI, in addition to the temporal profiles. The main results and possible differences to previous findings obtained under slightly different conditions and with a different additive are combined in a comprehensive picture in the discussion section, including also a brief outlook on the consequences of these results for technical applications, followed by a brief summary.

Results

Mg deposition on a Pt film electrode from BMP-TFSI based electrolytes

First we recorded cyclic voltammograms together with online mass spectrometric signals on a Pt film electrode in the four

Table 1. Composition of the different electrolytes used in this study.

Electrolyte	Solvent	$Mg(TFSI)_2$	$Mg(BH_4)_2$	18-c-6
I	BMP-TFSI	0.1 M	–	0.1 M
II	BMP-TFSI	–	0.1 M	0.1 M
III	BMP-TFSI	0.1 M	0.1 M	0.1 M
IV	BMP-TFSI	0.1 M	0.1 M	1.0 M

ChemElectroChem

Research Article
doi.org/10.1002/celc.202300090

Chemistry
Europe
European Chemical
Societies Publishing

different Mg-containing BMP-TFSI based electrolytes (see table 1). The Faradaic currents are presented as current-voltage plots in the Supporting Information (SI) in Figure S1 and discussed there in more detail. In summary, they show that reasonably stable cycling can be obtained for electrolytes III and IV, at least on the scale of the present experiments, but not for electrolytes I and II. The general trends in the CVs largely resemble those reported previously for a glassy carbon electrode in the same electrolytes[15] when considering the 50-fold lower scan rate, which results in much lower current densities and in particular in a much more pronounced passivation in the present CVs per scan, due to the more pronounced formation of inhibiting species.

In Figure 1 we show the time dependence of the potential, of the current density and of selected mass spectrometric ion currents during the first three (four in Figure 1d) potential cycles in the different electrolytes. Before these measurements, the sample was kept under open circuit conditions in this electrolyte for several hours (OCPs see at the different electrolytes).

For electrolyte I (0.1 M Mg(TFSI)$_2$ + 0.1 M 18-c-6, Figure 1a, final OCP value: 0.95 V), where the Mg^{2+} ions are coordinated to the TFSI$^-$ anion[28,29] and (predominantly) to the 18-c-6 ring,[27] the current is generally very low. When activating the potential control and stepping from the OCP to the positive potential limit, we find a small positive spike in the Faradaic current (inset in Figure 1a). Note that in the following we will describe this as a potential step to the positive potential limit. In contrast, the m/z = 2 (H$_2$) signal is essentially zero before, during and after the potential step in this borohydride-free electrolyte (Figure 1a). At potentials around the negative potential limit there is a small, but clearly resolved increase of the m/z = 2 ion current, indicating H$_2$ evolution. This occurs in parallel to the significant increase in Faradaic current density in this potential range. The asymmetric current peak shape (see also Figure S1a) indicates, however, that this peak is not only due to H$_2$ evolution, but also contains contributions from other irreversible processes. In the subsequent cycles, the H$_2$ signal remains at the noise level, which fits with the much smaller electrochemical current in these cycles. H$_2$ evolution can result from either reductive decomposition of the electrolyte and/or from reduction of trace impurities of water. Both are expected to lead to a passivation of the electrode, due to the formation of adsorbed electrolyte fragments and/or Mg (hydr)oxy species. The other ion currents depicted in Figure 1a are essentially featureless.

For electrolyte II (0.1 M Mg(BH$_4$)$_2$ + 0.1 M 18-c-6, Figure 1b, Figure S1b, final OCP value: ca. 0.6 V), the Faradaic current densities are much higher. Furthermore, we find a small oxidation current with a symmetric peak centered at ca. 0.25 V, which is likely due to Mg stripping. The apparent Coulombic efficiency of this process (compared to the cathodic current in the Mg deposition regime) is, however, still rather poor, indicating either irreversible deposition processes and/or a passivation of the electrode as dominant reductive processes. Also in this case the H$_2$ signal was essentially zero, i.e., at the background level before the potential step, but increases when

stepping from the OCP to the upper potential limit (see inset in Figure 1b). A similar increase is observed also for the Faradaic current, though on a lower scale than in electrolyte I, while the other signals do not change much. Both H$_2$ formation and Faradaic current decay rather quickly and almost reach the background level after 1000 s, at a potential slightly above 0.8 V. Here it is important to note that contributions to the Faradaic current resulting from capacitive charging are limited to the very initial phase, below 1 s.[12]

Obviously, an increase in the H$_2$ formation rate due to reductive H$_2$ formation fits neither with the initial increase in the oxidation current nor with the high anodic potential of around 0.8–1.0 V. This apparent discrepancy can be resolved in two different ways. In the first case, H$_2$ formation results from the well-known chemical bulk oxidation of borohydride by reaction with trace impurities of water[43] according to

$$BH_4^- + 2\ H_2O \rightarrow BO_2^- + 4\ H_2 \tag{1}$$

In addition to the formation of (insoluble) Mg borates along reaction (1), also the formation of hydroxylated species such as borotetrahydroxylates is possible, as described by eq. (1a)

$$BH_4^- + 4\ H_2O \rightarrow B(OH)_4^- + 4\ H_2 \tag{1a}$$
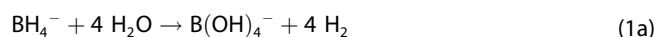
For simplification, we will assume in the following that this reaction leads to borate formation, although small contributions from hydroxylated species cannot be ruled out, though it would require twice as much water per borohydride anion. Such kind of bulk reaction should, however, have started already upon preparing/resting the electrolyte, and not only when stepping the potential. Since we have no indication for measurable H$_2$ evolution before the potential step, we can exclude that the sudden increase in H$_2$ evolution stems from reactions (1) or (1a). It is also rather unlikely because of the low concentration of water trace impurities.

A potential dependent H$_2$ evolution could result from the above reactions, however, if at least part of the evolving H$_2$ is electro-oxidized at sufficiently anodic potentials along the reaction in eq. (2):

$$H_2 \rightarrow 2\ H^+ + 2\ e^- \tag{2}$$

which could lower the measured H$_2$ signal. In that case, the strong increase could be due to a potential dependent, sudden decrease of the H$_2$ oxidation rate, for example, due to Pt oxidation. As demonstrated in previous studies, this reaction is indeed possible also in a variety of different RTILs, where the exact potential depends strongly on the nature of cation and anion.[44–46] Considering, however, the very low concentrations of the H$_2$O and/or O$_2$ trace impurities in these electrolytes and the rather small amount of H$_2$ formation by borohydride bulk oxidation detected in O$_2$-saturated and borohydride-containing electrolyte in the absence of a Pt electrode (see Figure 3a and related discussion), the H$_2$ signal expected from the borohydride bulk reaction in the present electrolyte should be well below the detection limit of these DEMS measurements. There-
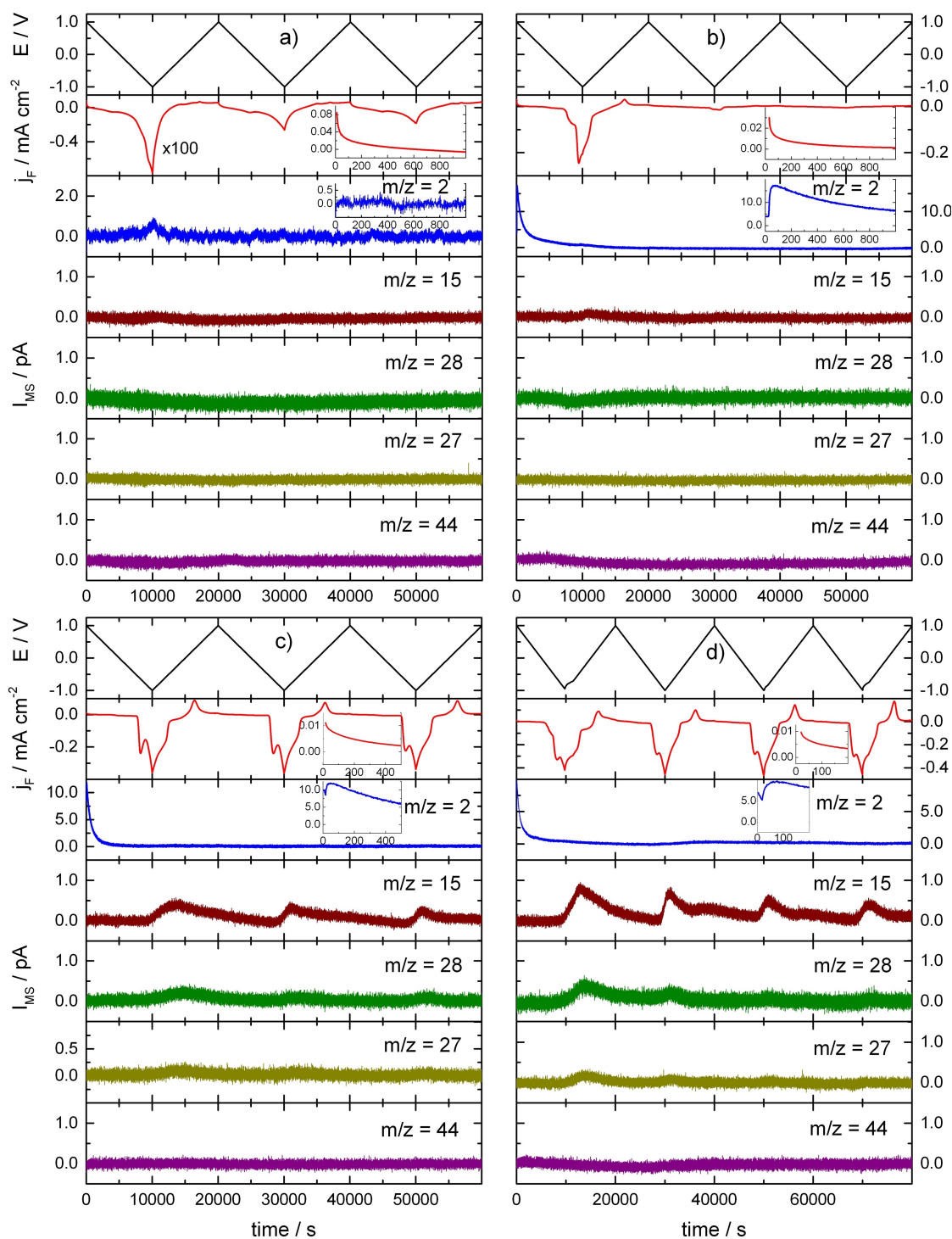
Figure 1. Time-resolved profiles of the electrode potential, Faradaic current density, and selected ion currents (for assignments see figure) recorded during cyclic voltammetry on a Pt film electrode (Figure S1) in BMP-TFSI based electrolytes I–IV, containing: 0.1 M Mg(TFSI)$_2$ + 0.1 M 18-c-6 (a), 0.1 M Mg(BH$_4$)$_2$ + 0.1 M 18-c-6 (b), 0.1 M Mg(TFSI)$_2$ + 0.1 M Mg(BH$_4$)$_2$ + 0.1 M 18-c-6 (c), and 0.1 M Mg(TFSI)$_2$ + 0.1 M Mg(BH$_4$)$_2$ + 1.0 M 18-c-6 (d). Potential scan rate 0.2 mV s^{-1}, room temperature, Mg foil stripe counter and reference electrodes. The insets show the Faradaic current density and the m/z = 2 ion current transients, respectively, during the initial time period.

fore, the pronounced increase in the H$_2$ signal upon stepping to the positive potential limit cannot be due to the combination of a potential independent borohydride bulk oxidation reaction and a potential dependent H$_2$ consumption due to H$_2$ oxidation. From the same reason, Faradaic currents arising from the

oxidation of H$_2$ created via the bulk reaction of borohydride with trace impurities of O$_2$ (eq. (1)) should be negligible. Note that the situation is different for higher concentration of O$_2$ or H$_2$O as, for example, in O$_2$-saturated electrolyte, which will be discussed later.

ChemElectroChem

Research Article
doi.org/10.1002/celc.202300090

**Chemistry
Europe**
European Chemical
Societies Publishing

Alternatively, H_2 formation could be possible via the (partial) electrocatalytic oxidation of borohydride according to eq. (3)

$$BH_4^- + 2\,H_2O \rightarrow BO_2^- + (8\text{-}x)/_2\,H_2 + x\,H^+ + x\,e^- \qquad (3)$$
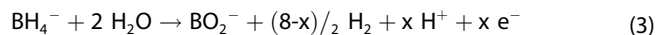
which for complete electrooxidation (x = 8) would result in the reaction (eq. 4)

$$BH_4^- + 2\,H_2O \rightarrow BO_2^- + 8\,H^+ + 8\,e^- \qquad (4)$$
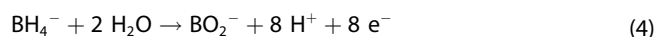
In the present case, where the potential step is expected to lead to Pt oxidation, we would expect mainly reaction (3), as reaction (4) is only possible on a reduced metallic Pt electrode (for details see Ref. [47]). These reactions had been reported for aqueous electrolytes, but have to be verified for reaction in organic electrolyte.[48–50]

Subsequently, upon lowering the potential, PtO reduction sets in and borohydride oxidation can occur via reaction (4), leading to a fast decay of the H_2 signal. The measured oxidation current seems to decay even faster, which may be due to an increasing contribution from the reduction of trace impurities of O_2 according to the reaction in eq. (5)

$$O_2 + e^- \rightarrow O_2^- \; (\text{or } O_2 + 2\,e^- \rightarrow O_2^{2-}) \qquad (5)$$
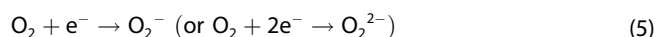
(see the Faradaic current in the inset in Figure 1b). At about 0.8 V, after about 1000 s, the situation experienced at the OCP (zero net Faradaic current and no measurable H_2 evolution, see insets in Figure 1b) is reached again. At about 0.25 V the reduction current (Mg^{2+} reduction and possibly electrolyte decomposition) starts, becoming more pronounced at about −0.25 V.

Overall, the data indicate that for the present electrolyte H_2 formation is dominated by electrooxidation of borohydride rather than by electrolyte decomposition. Note that small contributions to the Faradaic current from Pt surface oxidation and reduction were not considered in this discussion.

With further deceasing potential, we find a small peak in the m/z = 2 signal, possibly due to H_2 evolution via water reduction according to eq. (6)

$$2\,H_2O + 2\,e^- \rightarrow 2\,OH^- + H_2 \qquad (6)$$

parallel to the distinct reduction peak in the range between −0.5 V and the negative potential limit. Also the m/z = 15 ion current shows a small but distinct increase with the increasing reduction current (Figure 1b), smaller than in Figure 1a, which could tentatively be assigned to the reductive decomposition of electrolyte.

In the second cycle, there are no significant features visible any more in the Faradaic current and mass spectrometric signals, pointing to an efficient passivation of the electrode in the first cycle. In particular Mg stripping and Mg deposition peaks are almost completely absent in the second cycle. Nevertheless, the passivation must be less efficient in electrolyte II than in electrolyte I, considering the even lower Faradaic

current signal in Figure 1a. The absence of a H_2 evolution peak in the second cycle, in contrast, is no direct proof for an efficient passivation, as this may result also from a depletion of H_2O trace impurities in the first cycle. We tentatively explain the slight improvement in reversibility/passivation by the slower formation of inhibiting Mg oxy-species in electrolyte II, where the water scavenger BH_4^- species results in an efficient lowering of the level of H_2O and O_2 trace impurities.

Results of similar experiments in the electrolytes III (0.1 M $Mg(TFSI)_2$ + 0.1 M $Mg(BH_4)_2$ + 0.1 M 18-c-6, final OCP value: 0.4 V) and IV (0.1 M $Mg(TFSI)_2$ + 0.1 M $Mg(BH_4)_2$ + 1.0 M 18-c-6, final OCP value: 0.6 V), which contain a higher Mg^{2+} concentration as well as both additives, are plotted in Figure 1c and 1d. Most important, the current densities show an improved reversibility of Mg deposition and stripping (Figure 1c and 1d, Figure S1c and S1d). Nevertheless, the oxidation charge is still significantly lower than the reduction charge. As for electrolyte II (Figure 1b), both electrolytes result in a high initial H_2 formation rate at the upper potential limit, which decreases rapidly with decreasing potential, until reaching close to negligible values at ca. 0.5 V. The intensities are, however, somewhat lower than those in electrolyte II. Closer inspection of the Faradaic current (see insets in the two figures) reveals that similar to electrolyte II also in this case the potential step results in a small anodic current (about 10 μA cm^{-2}), which decays within 200–400 s, i.e., again on a much longer time scale than expected for capacitive charging. Also in this case the decay of the H_2 signal is slower than that of the Faradaic current, and there is still considerable H_2 evolution detected once the Faradaic current is negligible. As discussed above (Figure 1b), we relate the H_2 evolution under these conditions to a combination of partial electrochemical borohydride oxidation by reaction with trace impurities of water (reaction (3)), and PtO reduction. In subsequent cycles, H_2 formation is not observed any more. While the somewhat lower H_2 signals compared to electrolyte II and the absence of these signals in the second and third cycle may result also from lower levels and depletion of the H_2O trace impurities rather than from surface passivation, the much more pronounced Faradaic current signals in the second and third cycle clearly indicate an improved reversibility/lower passivation. This is most likely related to the higher concentration of Mg^{2+} in electrolytes III and IV compared to electrolyte II. Most simply, due to the limited amount of H_2O trace impurities a smaller fraction of the Mg^{2+} is converted into Mg oxy-species, increasing the probability for reversible Mg deposition/stripping and thus the reversible Mg deposition/stripping charge as compared to electrolyte I and II. Furthermore, we find a clear variation for the m/z = 15, m/z = 28 and even m/z = 27 signals with electrode potential in the mixed electrolytes ($Mg(TFSI)_2$ and $Mg(BH_4)_2$) in Figures 1c and 1d, in contrast to the very small increase of the m/z = 15 signal in Figure 1b and the essentially featureless other ion currents (except for H_2) in Figures 1a and 1b. These signals are typical for fragments resulting from the electron impact ionization of light hydrocarbons such as methane or ethene.[51] They are likely to originate from the decomposition of 18-c-6 upon the reduction of its complex with Mg^{2+} ions, and are

ChemElectroChem

Research Article
doi.org/10.1002/celc.202300090

Chemistry
Europe
European Chemical
Societies Publishing

detected at higher Mg^{2+} concentrations. Borohydride can be ruled out as source for the m/z = 15 signal, since evaporation as BH_4^- anion from the electrolyte is impossible. Mg-induced decomposition of $TFSI^-$, as proposed in references,[13,15] appears to be less likely under these conditions, since compared to electrolytes I and II their concentration hardly changed and they are present in large excess. Also, 18-c-6 is expected to more strongly complex Mg^{2+} ions than $TFSI^-$,[15] reducing the tendency for Mg-induced decomposition of $TFSI^-$ in electrolytes III and IV. Considering the structure of 18-c-6 one may expect ethylene oxide formation upon splitting the ring to fragments. However, the fragmentation pattern of ethylene oxide, where the m/z = 44 intensity should nearly be equal to that of m/z = 15,[51] does not fit to the relative intensities of the m/z = 15, m/z = 27, and m/z = 28 ion currents and to the rather featureless m/z = 44 signals in these figures. As another possibility, one might expect the formation of ethene (the featureless m/z = 30 signal (not shown) excludes ethane formation). Ethene formation had indeed been reported by Hegemann et al. upon stripping of Mg electrodeposited from a Magnesium Aluminum Chloride Complex (MAAC)-tetraglyme electrolyte,[52] which is rather similar to the crown ether used here as additive, since the 18-c-6 can be considered as a cyclic glyme. Those authors also proposed that decomposition of tetraglyme to ethene should be induced by electrons released upon Mg stripping. This, however, does not fit with the present observation of ethene formation upon Mg electrodeposition only at potentials well below Mg stripping, leaving questions for the underlying mechanism still open. Furthermore, ethene formation should result in a dominant m/z = 28 signal, a relatively high m/z = 27 signal and a rather low m/z = 15 intensity,[51] which differs from the ratio of these intensities in the experimental data. Therefore, there must be additional evolution of methane to reach a higher m/z = 15 signal, which requires C—C bond splitting of the 18-c-6 ring, in addition to C—O bond breaking. Apparently, reduction of Mg^{2+} in the complex with 18-c-6 leads also to some reductive decomposition of 18-c-6, for example, via ring opening. The higher amount of 18-c-6 decomposition in electrolyte III and IV as compared to the other ones seems to be correlated with the higher Mg^{2+} concentration in the electrolytes, which also leads to more efficient Mg^{2+} reduction. Interestingly, after setting in at the lower potential limit, the gas evolution at m/z = 15, 27, and 28 continues and is tailing over the entire positive-going scan, which means that these fragments are most likely formed via immobilized intermediate species, which then decompose slowly with time in a chemical reaction.

The present proposal of a 18-c-6 ring opening upon the reduction of its complex with Mg^{2+} extends previous proposals of a Mg-induced decomposition of $TFSI^-$ upon reduction of Mg^{2+} in a Mg-TFSI complex.[17,27–29,33,35] It fits well, however, with other previous reports, where based on laser infrared multiple photon dissociation (IRMPD) spectroscopy in combination with DFT calculations the authors concluded that in the most stable conformers, where the 18-c-6 ring nearly completely surrounds the Mg^{2+} ion, the crown ether ring is already opened.[53] While $TFSI^-$ decomposition during Mg^{2+} reduction was demonstrated

already in recent quantum chemical calculations,[15,25] the present data furthermore show that also complexation with 18-c-6 is not fully stable, but can result in a decomposition of the crown ether upon reduction, which had not been considered before. Nevertheless, the significantly enhanced reversibility of Mg deposition/Mg stripping in electrolytes III and IV clearly indicates that the decomposition of the 18-c-6 crown ether has much less effect on the passivation process than the $TFSI^-$ decomposition and deposition of Mg oxy-species in the electrolytes I or II, respectively. The latter processes must be slowed down in electrolytes III and IV.

Overall, these measurements have shown that for an efficient Mg deposition from different BMP-TFSI based electrolytes both 18-c-6 and borohydride are necessary, in agreement with the data reported in Ref. [15]. The mass spectrometric data furthermore indicated that in the absence of borohydride (electrolyte I), the small reduction current mainly arises from side reactions such as the evolution of H_2 from the electro-reduction of trace amounts of water (reaction (6)) and the decomposition of the electrolyte components. This leads to a rapid passivation of the electrode, which was not evident from our previous, purely electrochemical measurements.[15] In borohydride containing electrolytes (II–IV), where the reduction currents are significantly higher, this is explained by the removal of trace impurities such as water by reaction with borohydride, by slow chemical bulk reaction in the electrolyte before the electrochemical measurements and/or by electro-oxidation upon cycling, where the latter is indicated by potential dependent H_2 evolution. This improves the reversible Mg deposition/stripping, as confirmed by the appearance of Mg stripping peaks in the positive-going scan in these electrolytes (II–IV). There are also distinct Mg^{2+} concentration effects, since in electrolytes III and IV with their twofold higher Mg^{2+} concentration $(Mg(TFSI)_2 + Mg(BH_4)_2)$, the long-term reversibility is much better than in electrolyte II with its lower Mg^{2+} concentration (only $Mg(BH_4)_2$). While in electrolyte II a stripping peak is only observed in the first cycle, but not in subsequent ones, these increase in the other two electrolytes during subsequent cycles. As another major new finding, we find a measurable degradation of the 18-c-6 additive during Mg deposition, as indicated by ethene formation, which should go along also with an enhanced formation and deposition (see next section) of other decomposition products. While this is only visible for electrolytes III and IV with their higher Mg^{2+} concentrations, we expect this to occur also in the other electrolytes, but at a lower rate. Obviously, this improves the sustained reversibility of Mg deposition/dissolution upon cycling, though a detailed understanding of the underlying effects is still missing. Finally, the observation of an improved reversible Mg deposition/stripping upon addition of borohydride as additive agrees also with the previous report of an improved Mg (de−)intercalation in a Chevrel-type electrode from a DME-based electrolyte.[54]

ChemElectroChem

Research Article
doi.org/10.1002/celc.202300090

Chemistry
Europe
European Chemical
Societies Publishing

SEM/EDS characterization of Mg electrodeposits on a Pt film electrode from BMP-TFSI based electrolytes

Further information about the Mg deposition process and the nature of the deposits was obtained from SEM images and EDS maps, which were recorded after potential cycling as described in Figure 1, plus sample storage in a glove box. Figure 2 depicts the surface morphologies (upper two rows) and the elemental composition (lower rows) of the surface regions of the electrodeposits obtained on the Pt film electrode in the different electrolytes, respectively. Images of the element-specific distribution of Mg, O, F and C in the area presented in the upper row are shown in the bottom two rows of Figure 2. Quantitatively, the EDS results are summarized in Table 2.

Some general trends for the Mg electrodeposition can already be derived from the SEM images. Hardly any visible deposit can be identified after deposition from electrolyte I (0.1 M Mg(TFSI)$_2$ + 0.1 M 18-c-6, Figure 2a) at the present scale. Except for a guiding artifact of a damaged Pt film substrate in the middle part of the SEM image in Figure 2a, the surface is smooth and without resolved structures, similar to the pristine Pt film. At ca. tenfold higher magnification (Figure 2b) one can

resolve a few aggregates and small structures, in addition to cracks in the Pt film. The small structures can be attributed to Mg particles whose further growth was inhibited by the deposition of a passivating layer of electrolyte fragments and Mg (hydr)oxides that were formed already during the first deposition scan.[40,41] There is little evidence for Mg deposition in this electrolyte, and also the passivating layer formed during deposition is not really resolved. These conclusions are supported by EDS elemental maps recorded at the same location as the SEM images (Figure 2c1–2c4), which show predominantly Pt (30.6 at.%) and especially C species (52.0 at.%), less O and F (7.8 and 6.8 at.%), while other elements are below 2 at.%. Carbon, oxygen, fluorine and trace amounts of sulfur may originate from BMP-TFSI traces on the surface or from BMP-TFSI decomposition products. Carbon and oxygen can also reflect residues from 18-c-6 decomposition and surface contamination picked up during transport through air, while Mg (hydr)oxide formation must be less important. These species are homogeneously distributed over the surface, except for a few defect structures, which are also visible in the SEM images.

For electrolyte II (0.1 M Mg(BH$_4$)$_2$ + 0.1 M 18-c-6, Figure 2d–2f) we find a closed deposit layer on the Pt film substrate
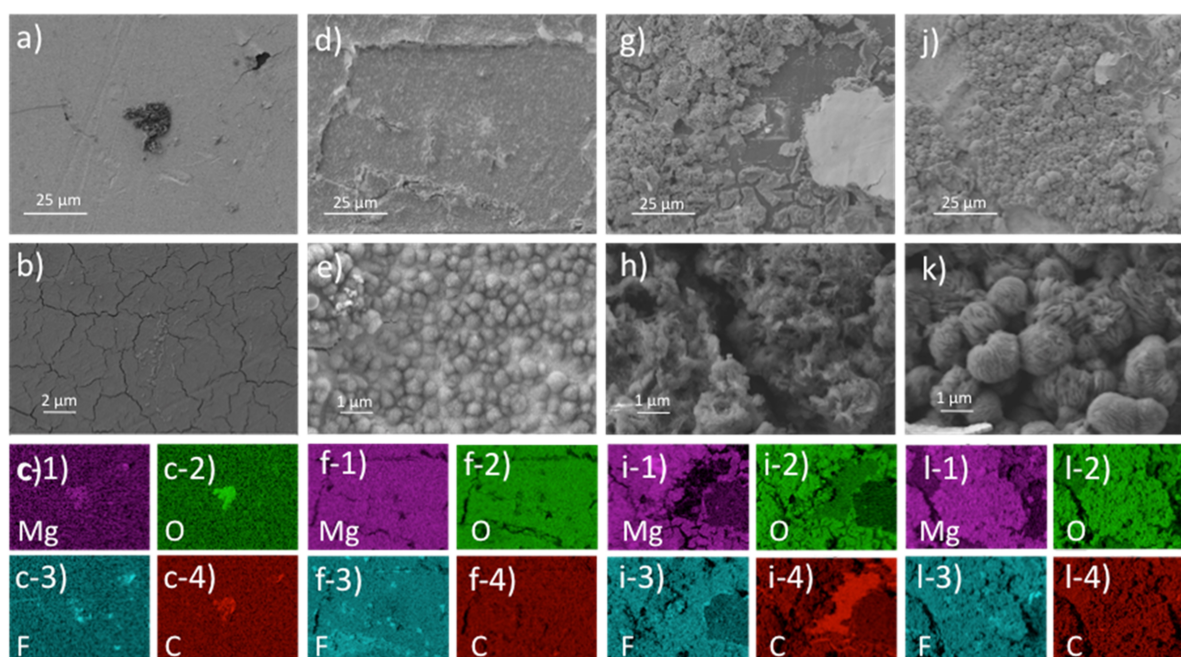
Figure 2. SEM (upper two rows) images at different magnifications and element specific EDS maps for Mg, O, F and C (same area as topmost row) of the electrodeposits formed after cyclic voltammetry of a Pt film electrode in neat, BMP-TFSI based electrolytes I–IV, containing: 0.1 M Mg(TFSI)$_2$ + 0.1 M 18-c-6 (a–c), 0.1 M Mg(BH$_4$)$_2$ + 0.1 M 18-c-6 (d–f), 0.1 M Mg(TFSI)$_2$ + 0.1 M Mg(BH$_4$)$_2$ + 0.1 M 18-c-6 (g–i), and 0.1 M Mg(TFSI)$_2$ + 0.1 M Mg(BH$_4$)$_2$ + 1.0 M 18-c-6 (j–l).

Table 2. Elemental surface composition of the electrodeposits formed on the Pt film electrode in the corresponding BMP-TFSI electrolytes I–IV, based on the EDS measurements in Figure 2. Data are averaged over the upper row images, relative deviations due to local variations are estimated to be ±3%.

Electrolyte	at.%							
	Pt	Mg	O	C	F	S	N	B
I (Figure 3c)	30.6	1.7	7.8	52.0	6.8	1.2	–	–
II (Figure 3f)	3.5	15.6	40.7	23.0	13.3	1.2	–	2.9
III (Figure 3i)	2.4	13.9	21.3	46.9	11.6	1.8	2.2	–
IV (Figure 3l)	3.1	22.2	30.9	27.3	13.3	1.2	0.8	1.3

ChemElectroChem

Research Article
doi.org/10.1002/celc.202300090

Chemistry
Europe
European Chemical
Societies Publishing

(Figure 2d), consisting of fused, sub-micrometer size hemispherical particles, as resolved at ca. 20-fold higher resolution (Figure 2e). The morphology of the Mg deposit differs from previous findings for magnesium deposition on a Pt electrode from a Grignard reagent based electrolyte,[55] where compact, hexagonally shaped particles with a uniform size of approximately 2–3 μm were observed, indicating a different Mg growth behavior in the present electrolyte. The observation of significant Mg deposition agrees fully with the much lower intensity of the Pt substrate signal (3.5 at.%) and the ca. tenfold higher Mg content (Table 2) compared to deposition from electrolyte I. Furthermore, the higher amounts of F and in particular O point to an enhanced deposition of Mg oxy-species and increased presence of TFSI species/fragments, resulting either from remaining electrolyte traces on the surface or from increased deposition of electrolyte fragments. Contributions from 18-c-6 decomposition products such as (oligo−)polymeric ether species, which may be expected, cannot be high based on the much lower carbon concentration. Finally, the observation of B-containing species, most likely borates, can be explained either by their formation during reaction in the experiments or by reaction of electrolyte traces on the emersed samples with O_2 or H_2O during storage/transport to the SEM. In total, these data fully agree with the conclusions derived from the DEMS measurements that Mg deposition from BMP-TFSI based electrolyte is possible in the presence of borohydride (and 18-c-6), while in its absence (electrolyte I) this is inhibited.

The electrodeposit formed upon deposition from electrolyte III (0.1 M $Mg(TFSI)_2$ + 0.1 M $Mg(BH_4)_2$ + 0.1 M 18-c-6, Figure 2g–2i) results in a film of approximately similar total thickness as in electrolyte II, as indicated by the comparable EDS signal from the Pt substrate (see below). In contrast to the rather regular hemispheric structures formed in electrolyte II (Figure 2e), the electrodeposit obtained in electrolyte III exhibits relatively large, irregular agglomerates (Figure 2h). Some of them have cauliflower-like morphologies, similar to those reported for the Mg electrodeposits from BMP-TFSI based electrolyte in the presence of O_2.[11,14] The structures resolved here differ from the mossy, non-dendritic morphology of the electrodeposits reported previously for deposition from a mixed $Mg(TFSI)_2$, 18-c-6 and MPPp-TFSI electrolyte (molar ratio 0.32:0.32:1.6 M),[27] where the mossy shape was attributed to the inclusion of organic fragments and impurities in the plated Mg.[27] Overall, the RTIL based electrolytes result in a different growth behavior compared to the more dendritic growth in Grignard based electrolytes.[56] EDS measurements (Figure 2i) show a comparable amount of Mg deposit as for deposition from electrolyte II, further supporting our previous conclusion that Mg deposition in electrolyte III is similarly efficient as in electrolyte II. The O content, however, is only half of that in electrolyte II, while the C content is more than doubled (Table 2). Since the amounts of F and S originating from the residual BMP-TFSI/TFSI fragments are comparable to those obtained in electrolyte II (Table 2), the higher amount of carbon in the present deposit points to an enhanced formation and deposition of 18-c-6 decomposition products. This would

correlate with the higher mass spectrometric signals for the 18-c-6 decomposition (alkane/alkene fragments) (Figure 1c).

Finally, the electrodeposit obtained from the electrolyte IV with its higher 18-c-6 concentration (0.1 M $Mg(TFSI)_2$, 0.1 M $Mg(BH_4)_2$, 1.0 M 18-c-6, Figure 2j–2 l) shows again hemispherical particles (Figure 2j), which in higher resolution images (Figure 2k) reveal a distinct microstructure with fibers running in parallel to each other. Mg electrodeposits with comparable morphologies have been reported also for deposition from a so-called "hybrid electrolyte", consisting of a mixture of BMP-TFSI and tetraglyme at a molar ratio 1:2, with both $Mg(TFSI)_2$ and $Mg(BH_4)_2$ salts, which showed an extraordinary reversible Mg deposition and stripping on glassy carbon electrodes.[56] Since an XRD analysis of those deposits showed a dominant Mg growth along the (100) orientation, which was also supported by a theoretical study,[57] one may speculate that similar effects happen also in the present case.

The elemental composition of this electrodeposit shows a comparable Pt intensity and a significantly higher Mg intensity compared to deposition from electrolytes II and III, supporting our previous conclusion that the higher concentration of 18-c-6 improves Mg deposition. In addition, also the oxygen intensity increases significantly, while that of carbon decreases considerably, and the other signals do not change much. The presence of F, S, N and B again points to residues from the electrolyte and BMP-TFSI decomposition, whereas the higher concentration of O stands for the enhanced formation of Mg oxy-species and possibly 18-c-6 decomposition products such as (oligo−)polyethers, which are formed upon Mg^{2+} reduction.

Overall, the SEM and EDS data support our conclusions from the CV/DEMS data. Significant Mg deposition is possible only in the presence of both borohydride and 18-c-6, while in the absence of one of these species it is negligible. Furthermore, they are compatible with the formation of Mg oxy-species during Mg deposition, as indicated by the simultaneous presence of Mg and O. Finally, in all of these electrolytes Mg deposition results in the formation of organic overlayers, confirming our previous conclusions in Ref. [15]). These contain either TFSI⁻ decomposition products and/or traces of electrolyte, and presumably 18-c-6 decomposition products. Traces of borates are also present, which may be formed either during reaction in the experiment or by reaction of borohydride in remaining electrolyte traces with the atmosphere during storage/transport of the emersed samples.

O_2 interaction with a Pt film electrode under open-circuit conditions in Mg^{2+}-containing, O_2-saturated BMP-TFSI based electrolytes

To explore the impact of O_2 in the electrolyte on the nature of the Mg deposit and the passivation of the electrode, we performed DEMS measurements on the interaction of O_2 with the Pt film electrode in the three BMP-TFSI based electrolytes I–III (Table 1) under open circuit conditions.

Before presenting and discussing these results, we will briefly discuss results of a test on possible contributions from a

ChemElectroChem

Research Article
doi.org/10.1002/celc.202300090

Chemistry Europe
European Chemical
Societies Publishing

chemical bulk reaction between borohydride and O_2, employing the same DEMS cell as used before, but a Pt-free FEP membrane inlet. Here we monitored changes in different mass signals when starting O_2 bubbling in a borohydride containing electrolyte (BMP-TFSI+0.1 M Mg(BH$_4$)$_2$).

O_2 bubbling leads to a distinct increase of the m/z=32 (and m/z=16) signal, but also to an increase of the m/z=2 signal (Figure 3a). The latter signal, which is indicative of H_2 formation, starts even prior to the increase of the m/z=32 signal. We attribute this to a chemical bulk reaction between borohydride and O_2, as given, for example, by the equation (7)
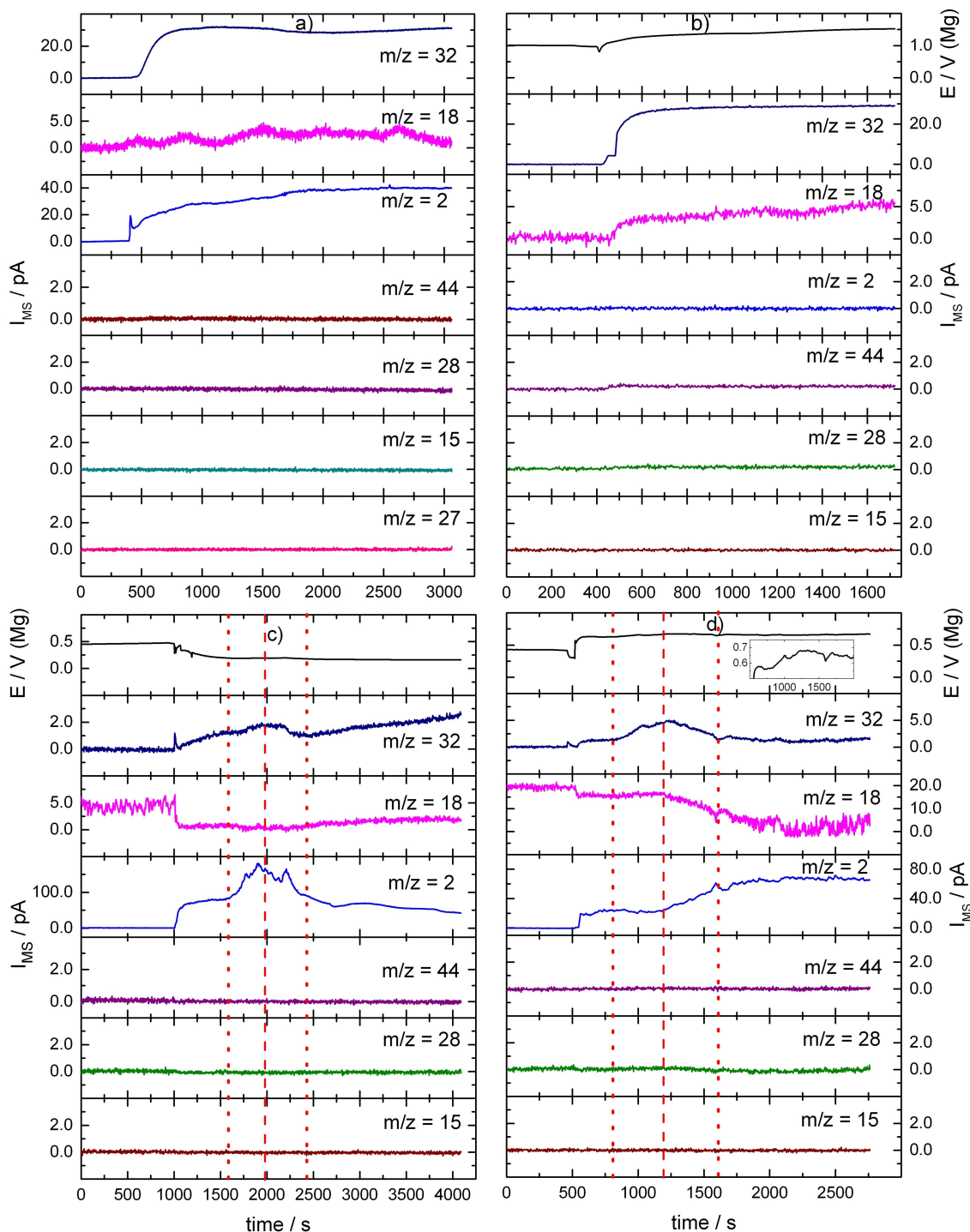
Figure 3. Time-resolved profiles of different ion currents (for assignments see figure) for a bare, Pt-free FEP membrane (a), and for a Pt film electrode sputtered onto the FEP membrane (b-d) before and during O_2 bubbling in different electrolytes (operation at open circuit potential). All measurements were performed in BMP-TFSI based electrolyte containing a) 0.1 M Mg(BH$_4$)$_2$, (b) 0.1 M Mg(TFSI)$_2$+0.1 M 18-c-6 (electrolyte I), c) 0.1 M Mg(BH$_4$)$_2$+0.1 M 18-c-6 (electrolyte II), and d) 0.1 M Mg(TFSI)$_2$+0.1 M Mg(BH$_4$)$_2$+0.1 M 18-c-6 (electrolyte III)). The dotted vertical lines in Figure 3c and 3d indicate the onset and end of the transient variations, the dashed vertical line marks a characteristic point therein (see text).

ChemElectroChem

Research Article
doi.org/10.1002/celc.202300090

Chemistry
Europe
European Chemical
Societies Publishing

$$BH_4^- + O_2 \rightarrow BO_2^- + 2\ H_2 \qquad (7)$$

The significant delay between starting the O_2 bubbling (= onset of the increase in the H_2 signal) and the onset of the O_2 signal indicates that during this time the gaseous O_2 in the vicinity of the membrane is completely consumed by the chemical bulk reaction between O_2 and borohydride. There are no measurable changes in the signals related to CO_2 formation ($m/z=44$ and 22) and alkene formation ($m/z=15, 27, 28$), and the water related ion current ($m/z=18$) shows only ill-defined bubbling-induced variations. Obviously, the chemical reaction between borohydride and O_2 is rather efficient under these conditions, as indicated, for example, by the observed H_2 evolution. It should be noted that in the presence of trace impurities of water also the formation of borohydroxides is possible, for example, via reaction (8)

$$BO_2^- + 2\ H_2O \rightarrow B(OH)_4^- \qquad (8)$$

To the best of our knowledge, these bulk reactions, specifically reaction (7), have not been considered so far for organic solvents or ionic liquids. Besides mitigation of O_2 formation and production of H_2, such chemical reactions will also result in the formation of borates. Furthermore, in the presence of Mg^{2+} ions, O_2 bubbling can also result in the formation of insoluble $Mg(OH)_2$ in the solution, via the reaction (9)

$$O_2 + 2\ H_2O + 4\ e^- \rightarrow 4\ OH^- \qquad (9)$$

The formation of insoluble species such as $Mg(OH)_2$ or $Mg(BO_2)_2$ is indicated also by the appearance of white colloidal aggregates in the formerly transparent solution of $Mg(BH_4)_2$ after O_2 bubbling.

Next, we monitored the response of the potential and the evolution of gaseous products upon O_2 bubbling under open circuit conditions, using a similar Pt film electrode as in the experiments to Figure 1. Figure 3b–3d shows chronopotentiometric transients (upper panels) and the corresponding chronoamperometric ion current transients before and after starting bubbling the electrolytes with O_2 (lower panels), where the onset of O_2 bubbling is indicated by the sudden increase in the O_2 signal ($m/z=32$).

Starting with electrolyte I (0.1 M $Mg(TFSI)_2$ + 0.1 M 18-c-6, Figure 3b), where the open circuit potential (OCP) value of the Pt film electrode before introducing O_2 is about 1.0 V, the OCP slowly increases by ca. 0.5 V upon admission of O_2 (at ca. 400 s, see the small spike in the potential). The increase of the OCP upon O_2 bubbling is attributed to an oxidation of the electrode surface. More detailed information will be gained from the ion current transients recorded simultaneously (Figure 3b–3d, lower panels). Upon O_2 admission, the $m/z=32$ ion current increases rapidly. Different from the situation in Figure 3a, there is no delay between O_2 admission and increase in O_2 signal, as there is no pathway for efficient O_2 consumption in this electrolyte. The additional structure in the initial phase of this signal in

Figure 3b is due to an experimental artifact, caused by saturation of the signal at ca. 450 s, while from ~500 s the signal was followed on a less sensitive scale. Within about five minutes after the onset of O_2 purging the signal reached a nearly constant value. Hence, at this point the electrolyte is saturated with O_2. This behavior fits to the increase of the OCP value discussed above. A slight increase of the $m/z=18$ signal is again explained by an enhanced convective transport of water traces to the electrode upon O_2 bubbling, whereas the small increase of the $m/z=44$ and $m/z=28$ ion currents is likely due to the oxidation of organic residues adsorbed on the electrode at the increasing OCP value. The $m/z=2$ and $m/z=15$ ion currents finally remained at their initial level.

In the borohydride containing electrolytes II and III (Figure 3c, 3d), the OCP is about 0.5 V lower before the onset of O_2 bubbling than in electrolyte I (Figure 3b). This lower value is most easily explained by the formation of a mixed potential, resulting from the simultaneous oxidation of borohydride to borate (reactions (3) and (4)) and the reduction of trace impurities of O_2 (reaction (5)) and/or water (reaction (6)) after filling the electrolyte into the cell. Furthermore, reduction of an oxide layer on the Pt electrode by the strongly reducing borohydride may also play a role. Upon O_2 admission, the OCP response differs significantly from that in electrolyte I. In electrolyte II, the potential decreases by ca. 0.25 V (Figure 3c), while in electrolyte III, where both $Mg(TFSI)_2$ and $Mg(BH_4)_2$ are present, it increases by ca. 0.25 V (except for a brief excursion to lower values directly during the switch). Furthermore, these changes occur significantly faster than in electrolyte I, in particular in electrolyte III. Reasons for these differences in the OCP behavior will be discussed together with the changes in mass spectrometric signals upon O_2 admission, which are presented in Figure 3c and 3d.

For electrolyte II (Figure 3c), there is only a slow continuous increase of the $m/z=32$ ion current, despite of O_2 bubbling, which contrasts the rapid increase in electrolyte I (Figure 3b). Also in this case there is no delay between H_2 formation (O_2 admission) and the increase in O_2 signal, despite the presence of BH_4^-. Obviously, different from the situation in Figure 3a, O_2 was not completely consumed by the bulk oxidation of borohydride (reaction (7)) in the initial phase, directly after O_2 admission, and therefore we see a small but measurable immediate increase in the O_2 signal at this point. Next, the $m/z=18$ signal decreases abruptly as opposed to the increase in Figure 3b, and there is a pronounced, instantaneous increase of the $m/z=2$ signal (H_2 evolution), followed by a slow decrease at later time. This contrasts the featureless $m/z=2$ current trace in Figure 3b. For all three signals we see an additional transient structure in the time between about 500 and 1500 s after the onset of O_2 bubbling, which we will get back to when discussing the behavior in electrolyte III (Figure 3d). Finally, the ion currents $m/z=44$, $m/z=28$ and $m/z=15$ remain unchanged.

We postulate that the admission of O_2 increases the tendency for the ORR (reaction (5)) and the electrocatalytic oxidation of borohydride via reactions (3) and (4), which in the absence of O_2 purging occurred at low rates. Under OCP

ChemElectroChem

Research Article
doi.org/10.1002/celc.202300090

Chemistry
Europe
European Chemical
Societies Publishing

conditions, these reactions must result in a zero net current. Upon admission of O_2, the drastic increase in O_2 concentration will also lead to a corresponding increase of the borohydride bulk oxidation rate according to reaction (7), which in turn results in a significant rate of H_2 formation. Simultaneous H_2 electro-oxidation (reaction (2)) does not seem to occur at these potentials, as in that case the H_2 signal should be lower than for the Pt-free membrane (Figure 3a), which is not the case. Therefore, we expect that the main partial reactions contributing to the mixed potential formation are the BOR and the ORR.[58] In combination, these data indicate that the compensation of electron-generation and consumption due to electro-oxidation and electro-reduction reactions before and after the admission of O_2 results in a shift of the OCP (mixed potential formation). The correlated sudden decay in the water signal, which is in contrast to the essentially constant signal on the Pt-free membrane, indicates that the traces of water in borohydride containing solution are consumed at the OCP only in the presence of the Pt film. This points to the participation of interfacial reactions in H_2O removal, for example, via reactions (3) and (4) in the present case. Finally, contributions from the ORR (reaction (3)) should be small at these OCP values (0.5→0.25 V, see Figure 3c). Another plausible cathodic partial reaction instead of the ORR in non-aqueous electrolyte (Eq. (5)), which involves both the consumption of O_2 and H_2O trace impurities, is given by reaction (9). This can lead to the formation of OH^- and thus, in the presence of Mg^{2+} in the solution, to $Mg(OH)_2$.

In electrolyte III (Figure 3d), the general trends are rather similar to those in electrolyte II, with the main differences that the OCP increases rather than decreases upon O_2 bubbling, that all changes upon O_2 bubbling are smaller and that for longer times the consumption of O_2 and H_2O, and the formation of H_2 do not co-decrease, but approach a saturation value. The different trend in OCP variation must be related to the higher Mg^{2+} concentration, since in both electrolytes we have borohydride present and the twofold higher Mg^{2+} concentration in electrolyte III is the only major difference. Most simply, this can be explained via deposition of Mg oxy-species, which affects the activity of the Pt surface such that H_2 electro-oxidation is more affected than O_2 reduction. In that case, admission of O_2 will lead to an increase in OCP, opposite to the behavior in electrolyte II. Here it should be noted that these shifts in OCP require only minute differences in the oxidation and reduction rates, respectively, as the resulting charges are accumulated with time.

Similar to electrolyte II, we also see same transient changes, here in the period between 700 and 1500 s after the onset of O_2 bubbling (see the dotted vertical lines in Figure 3d). In the first part of this period, up to the time indicated by the dashed vertical line, the O_2 signal is higher for some time, indicative of lower O_2 consumption, while the H_2O and H_2 signals remain constant and the OCP increases slightly (see the 10-fold magnified trace in this panel). Subsequently, the O_2 signal decreases again to the original level, and H_2O and H_2 signals irreversibly decrease or increase, respectively. While the initial decrease in O_2 consumption is likely due to the ORR, using

electrons provided by the incomplete oxidation of borohydride (reaction (3)), the increasing H_2 formation and H_2O consumption starting at the dotted vertical line (at about 1200 s) point to an irreversible increase of borohydride (electro−)oxidation (reactions (3), (4) and possibly reaction (7)). For current neutrality (under OCP conditions), the above partial oxidation reactions are compensated by an increased O_2 reduction (ORR) via reactions (5) and (9). These variations are reflected by a small decay in the OCP (see inset in Figure 3d). The physical origin of these changes is not clear so far, but it should be of similar nature as that for the transient changes in Figure 3c in a similar time frame, supporting that these changes reflect reproducible changes in the surface chemistry, rather than artifacts that are induced, for example, by O_2 bubbling.

Overall, these findings, in particular the differences between the OCP and mass spectrometric responses to O_2 bubbling in the absence and presence of borohydride in the electrolyte, indicate that in borohydride-free electrolyte I, O_2 exposure under OCP conditions leads to Pt surface oxidation, which in turn results in an increasing OCP. In the borohydride containing O_2-saturated electrolytes II and III, O_2 admission results in a complex network of reactions. These include the bulk chemical oxidation of borohydride to borates, by reaction with O_2, as well as a number of electrocatalytic reactions, such as electro-oxidation borohydride and of the H_2 produced that reaction and the electro-reduction of O_2. Under OCP conditions, these reactions lead to the formation of a mixed potential. This situation is similar to that experienced in 'catalytic' borohydride oxidation in aqueous electrolytes, which is also characterized by simultaneous oxidation of borohydride, reduction of water to OH^- and H_2 formation.[47] As a practical consequence, one has to consider that the use of borohydride as additive will result in undesired H_2 evolution and a gradual mitigation of borohydride at the open circuit potential in realistic Mg batteries.

O_2 reduction and evolution on a Pt film electrode from Mg^{2+}-containing, O_2-saturated BMP-TFSI based electrolytes

After saturation of the Mg^{2+} containing BMP-TFSI based electrolytes with O_2 at the OCP (see Figure 3), we performed similar cyclic voltammetry measurements as described in Figure 1 under continuing O_2 bubbling. Again, we followed the Faradaic current density as well as different mass spectrometric signals simultaneously during potential cycling in the O_2-saturated electrolytes I–III. Experimentally, the procedure was similar to that described before, with the electrode potential stepped from the OCP to the upper potential limit. Also in these measurements, effects from O_2 reduction/evolution, Mg deposition/stripping and the formation of insoluble deposits due to electrolyte decomposition, Mg (hydr)oxide formation or borate formation and finally H_2 oxidation have to be considered. Again, small contributions to the Faradaic current from Pt surface oxidation/reduction are not considered in the discussion. For better comparison with literature data we again plotted the Faradaic current densities as current-voltage plots in the Supporting Information in Figure S2, they are discussed there in

ChemElectroChem

Research Article
doi.org/10.1002/celc.202300090

Chemistry
Europe
European Chemical
Societies Publishing

more detail. In summary, they show that reasonably stable reversible cycling performance can be obtained for electrolytes III and IV, at least on the scale of the present experiments, but not for electrolytes I and II. Furthermore, the general trends in the CVs largely resemble those reported previously for a glassy carbon electrode in similar electrolytes, but using dimethyl aminoborane as a water scavenger.[14] This underlines the importance of a reducing additive in combination with a sufficiently high Mg^{2+} concentration for preventing electrode passivation by oxy-species that are stable against re-oxidation, a precondition for sustained reversibility in the oxygen-saturated electrolytes.

In Figure 4 we show plots of the Faradaic current densities and of different ion currents as a function of time during the first three cycles. A presentation of the initial phase on an expanded time scale is given in Figure S3. These latter plots demonstrate that also on that time scale there are no significant changes in the signals directly after stepping to the upper potential limit, independent of the electrolyte (for details see Figure S3). Hence, for all electrolytes the potential before the potential step the OCP was close to that reached upon the potential step.

In O_2-saturated electrolyte I (0.1 M $Mg(TFSI)_2 + 0.1$ M 18-c-6, Figure 4a), we find an initially slow increase of the Faradaic reduction current at > 0.1 V, which is accompanied by a small increase of the m/z=32 current signal. At present we can only speculate that this subtle increase in the O_2 signal is related to the reductive removal of some deposits that were formed under OCP conditions and which affect the permeability of the membrane. The first reduction peak in the negative-going scan with its onset at ca. 0.0 V (see also Figure S2a) goes along with increasing O_2 consumption, as evidenced by the steep decay of the m/z=32 signal. This reaches its minimum at ca. 10000 s (~ -0.6 V), and remains about constant until reaching ca. 0.0 V in the backward scan. The sharp peak in the m/z=2 ion current, which coincides with the equally sharp reduction current peak, indicates that both result from a reduction reaction associated with H_2 formation such as reduction of H_2O trace impurities. We cannot exclude, however, contributions from a change in the ORR selectivity, from a 1-electron process to a 2-electron process, which would perfectly agree with our previous data.[12,14,59] Interestingly, a comparable H_2 evolution was not observed in the O_2-free electrolyte in this potential region (Figure 1a), indicating that the presence of O_2 activates the reductive hydrogen evolution from traces of water and possibly also from electrolyte components. This interpretation is supported also by the fact that both the Faradaic current peak and the H_2 signal were very small in later cycles, after depletion of trace impurities or passivation of the surface against electrolyte decomposition. Finally, there is a reproducible increase of the m/z=44 signal when approaching the upper potential limit of 1.5 V (Figure 4a), which parallels the small increase of the oxidation current at potentials positive of ca. 1.25 V (Figure 4a). These features are most likely due to the oxidation of adsorbed organic residues from electrolyte components. Due to the low intensities of these signals we cannot decide upon the origin of these species, since we do not have any indication of BMP-TFSI

decomposition or 18-c-6 decomposition under these conditions from the other DEMS signals.

Similar traces recorded in analogous DEMS measurements in electrolyte II (0.1 M $Mg(BH_4)_2 + 0.1$ M 18-c-6) are plotted in Figure 4b (see also Figure S2b). Different from the measurements in the O_2-saturated electrolyte I (Figure 4a), the m/z=32 current is initially close to zero, although the electrolyte is O_2-saturated, indicative of an efficient reactive O_2 removal at high potentials. Assuming that the O_2 signal at the upper potential limit reflects essentially the level of bulk oxidation of borohydride by reaction with O_2 (eq. (7)), the subsequent decay of this signal (at about 5000 s) can be associated with the increasing consumption of borohydride (reaction (7)) and, at potentials below 0 V, the onset of the ORR (reaction (5)). Furthermore, we find efficient H_2 evolution under these conditions. The H_2 signal decreases about exponentially with time and is essentially insensitive to the potential changes, which points to a potential independent bulk reaction such as that described by reaction (7). This will be discussed in more detail below. (Note also that this decay is much slower than the H_2 decay in Figure 1b and 1c.) With further decreasing potential and its increase in the backward-going scan, the O_2 signal is close to the zero level, indicating that bulk chemical O_2 consumption and ORR together result in essentially complete consumption of O_2. The ongoing ORR will contribute part of the cathodic current to the Faradaic current signal, while the remaining current fraction must come from electrolyte decomposition and/or H_2 evolution (see below). At the end of the reduction peak in the Faradaic current, the O_2 mass signal increases again, reflecting a decreasing O_2 consumption. Most simply, this can be explained by a complete decay of the electrochemical ORR rate, such that only O_2 removal by the bulk reaction (7) is left. The small positive peak in the Faradaic current and in the O_2 mass signal at about 0.1 V, which is better visible in the second cycle, is likely to reflect electrocatalytic O_2 evolution. Apparently, a small part of the oxy-species formed upon the oxygen reduction and immobilized at the electrode surface can be re-oxidized to O_2 in the positive-going scan. In the subsequent scans, this general scheme repeats, with the only difference that from scan to scan the O_2 signal in the positive potential range becomes higher, as if O_2 removal via the bulk chemical reaction with borohydride becomes less efficient with time. This explanation is also supported by the negligible Faradaic current in these potential ranges. The reactions proposed and discussed above also imply that the nature of the deposits formed in electrolyte II is different from that in electrolyte I, being mostly Mg oxy-species in the present case and mostly electrolyte decomposition products in electrolyte I. This also seems to agree well with our EDS observations in O_2-free electrolyte.

The (m/z=2) signal, which is characterized by a slow, about exponential decrease, reaches zero after about 40 000 s (~ 11 h). This decay is overlaid by some broad, weak features around the negative potential limit (Figure 4b). Most important, the distinct peak observed in electrolyte I at the first negative potential limit is essentially absent here. Also, there is no evidence for H_2 electro-oxidation at more positive potentials, as would be expected for a Pt electrode. In that case, the H_2 signal should be

ChemElectroChem

Research Article
doi.org/10.1002/celc.202300090

Chemistry Europe
European Chemical
Societies Publishing
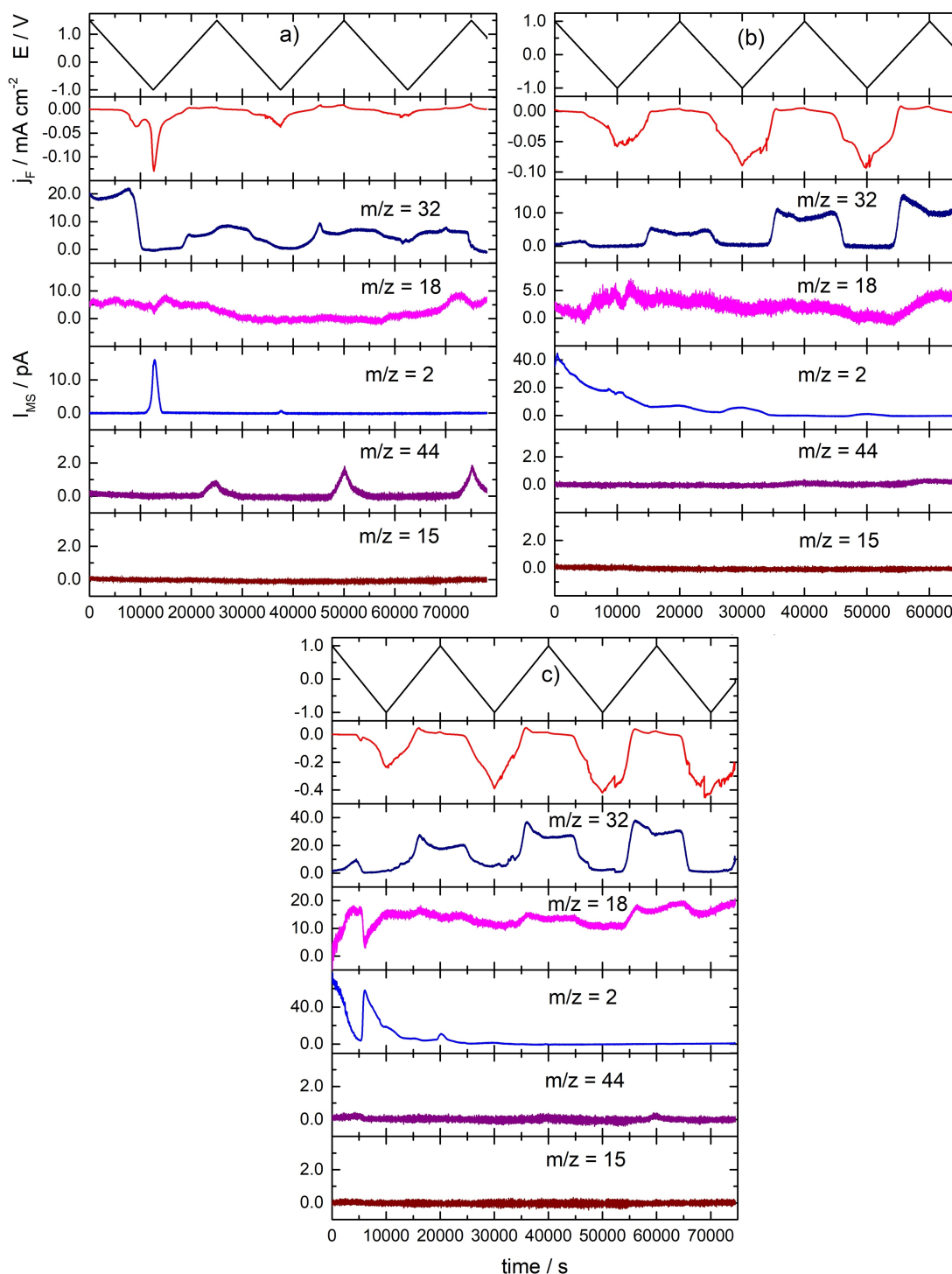
Figure 4. Time-resolved profiles of the electrode potential, Faradaic current density, and corresponding ion currents (for assignments see figure) during cyclic voltammetry on a Pt film electrode in the three different O_2-saturated BMP-TFSI based electrolytes I–III, containing: 0.1 M $Mg(TFSI)_2$ + 0.1 M 18-c-6 (a), 0.1 M $Mg(BH_4)_2$ + 0.1 M 18-c-6 (b), 0.1 M $Mg(TFSI)_2$ + 0.1 M $Mg(BH_4)_2$ + 0.1 M 18-c-6 (c). Potential scan rate 0.2 mV s^{-1}, room temperature, Mg foil stripe counter and reference electrodes.

much lower in the potential regime where this reaction is active. The weak features in the H_2 signal we tentatively attribute to either reductive electrolyte decomposition or to water reduction. The fact that they are much smaller than in electrolyte I supports our interpretation that in electrolyte I the

deposit consists mainly of electrolyte decomposition products, while in electrolyte II these are largely Mg oxy-species. The slow decrease of the H_2 signal, which is definitely related to the simultaneous presence of borohydride and O_2, is likely due to a gradual consumption of borohydride by bulk reaction with O_2

ChemElectroChem

Research Article
doi.org/10.1002/celc.202300090

Chemistry
Europe
European Chemical
Societies Publishing

(Eq. (7)). Here it is interesting to note that H_2 electrooxidation is apparently inhibited at more positive potentials, while O_2 reduction via the ORR is active at potentials below 0.0 V. Most simply, this can be explained assuming that the Pt surface was covered by Mg oxy-species already during the OCP phase in O_2-saturated electrolyte and that this cover layer is present also during potential cycling, at least at more positive potentials, and blocks the H_2 oxidation reaction. For the ORR this means that this reaction can proceed also on a surface covered by Mg oxy-species.

The other signals, including the $m/z=44$ and the $m/z=15$ ion currents (as well as the $m/z=27$ and $m/z=28$ signals, not shown) are essentially featureless in this electrolyte. We expect that the absence of CO_2 formation is mainly due to the lower value of the upper potential limit in this electrolyte (1.0 V rather than the 1.5 V in electrolyte I), which impedes oxidation of electrolyte decomposition products. Furthermore, the constant value of these signals is different from our observations in the absence of O_2, where these signals showed a distinct potential dependent structure, indicating that the crown ether is stable in the presence of O_2 and thus during O_2 reduction, but not in the absence of O_2. Most simply, this can be explained by the formation of insoluble Mg (per)oxy-species that remove Mg^{2+} from the complexes with 18-c-6, and thus lower 18-c-6 decomposition upon Mg^{2+} reduction.

Similar time-resolved profiles measured in the O_2-saturated electrolyte III (0.1 M $Mg(TFSI)_2 + 0.1$ M $Mg(BH_4)_2 + 0.1$ M 18-c-6) are plotted in Figure 4c (see also Figure S2c). Interestingly, the Faradaic current density is about four times larger than those obtained in electrolytes I and II (Figure 4a, 4b), which we relate to the higher Mg concentration. The general features are, however, rather similar. For the $m/z=2$ and $m/z=18$ signals, respectively, we find a rapid increase/decrease during the initial stage of the present experiment (at about 6000 s), which is caused by a re-adjustment of the O_2 bubbling rate. The general shape of the respective signal traces largely resembles those in Figure 4b. Therefore, they shall not be discussed again in detail. Main differences compared to electrolyte II are the more pronounced oxidative current peaks and peaks in the $m/z=32$ signal in the positive-going scans at about 0.15 V. (Note that also the small Faradaic current reduction peak at 5000 s (~ -0.1 V) in the first negative-going scan, which was not seen in Figure 4b, is attributed to the re-adjustment of the O_2 bubbling rate.) Hence, similar as in electrolyte II the potential controlled electrochemical reactions are accompanied by the bulk chemical reaction between O_2 and borohydride, which can continue until the latter is essentially depleted in the electrolyte. The more pronounced peaks at about 0.15 V point to a more efficient accumulation of oxidizable Mg oxy-species close to the electrode at more cathodic potentials, which is indicated also by the significantly higher ORR currents at more cathodic potentials (note the different scales in Figure 4b and 4c). This fully agrees with our conclusion of a more reversible ORR/OER and hence less pronounced passivation in this electrolyte as compared to electrolyte II (see the discussion of Figure S2c). It also agrees with previous findings by Eckardt et al. for the ORR/OER on a glassy carbon electrode in the same electrolyte,

though with a different additive.[14] In that work the ORR products in Mg^{2+}-containing BMP-TFSI were concluded to be MgO and MgO_2, where only the latter ones can be re-oxidized to form O_2.[14] Similar conclusions were reported also in earlier studies, based, e.g, on the number of electrons transferred per O_2 molecule.[12,42,59–61] Therefore, we assume that these species are formed also in the present case, where the latter can be re-oxidized to O_2 at 0.15 V.

To address the effects of O_2 bubbling and borohydride depletion upon O_2 bubbling in more detail, we performed a comparative experiment in electrolyte III where we used a longer time resting at the OCP with active O_2 bubbling (Figure S4a), followed by the ORR measurement (Figure S4b). As expected, we again find continuous H_2 formation during O_2 bubbling at the OCP, which is accompanied by only a slight increase in O_2 signal at the onset of O_2 bubbling (Figure S4a). Hence, there is a continuous consumption of O_2 during this time by bulk reaction with borohydride. During the subsequent potentiodynamic run, however, the H_2 formation rate decays much more rapid than in Figure 4c, concomitant with an increase of the O_2 signal. This fully agrees with expectations for a situation where most of the borohydride was already consumed during the waiting time at the OCP, and therefore cannot contribute to the overall reaction via reaction (7) any more. Except for the H_2 signal, the other signals show essentially similar trends during potential cycling as observed in Figure 4c. Comparable results were obtained also for test measurements performed with different O_2 bubbling rates, supporting the above conclusions.

Overall, the DEMS measurements in the different O_2-saturated Mg-containing electrolytes revealed that the reduction and oxidation currents contributing to the Faradaic current signal are a result of a complex combination of different reduction and oxidation processes that are going on at a given potential and that can (partly) compensate each other in the Faradaic current signal. The increasing reduction current at low electrode potentials, at about constant O_2 consumption, indicates a change in the ORR selectivity, from a 1-electron process to a 2-electron process. This would perfectly agree with our previous findings obtained in the BMP-TFSI based electrolyte in the absence of any additive,[12,59] or in the presence of the NBH additive,[14] which were all performed under well-defined mass transport condition in a thin-layer flow cell. The $m/z=32$ OER signals confirmed our previous observation that passivation of the Pt electrode is significantly lowered or even largely removed in the combined presence of both borohydride and 18-c-6 additives. This effect of a lower passivation is even more pronounced for the higher relative Mg^{2+} concentrations in electrolyte III, as indicated by the higher OER currents/O_2 signals compared to electrolyte II. For reaction in O_2-saturated borohydride containing solution we find reactions involving O_2, borohydride, 18-c-6, and water trace impurities as reactants. Furthermore, some of these reactions occur both as chemical bulk reaction and as electrochemical reaction, depending on the potential. The different contributions can be identified by comparison of Faradaic current, O_2 consumption/generation, water consumption and H_2 formation. Our conclusion of a

ChemElectroChem

Research Article
doi.org/10.1002/celc.202300090

Chemistry
Europe
European Chemical
Societies Publishing

considerable bulk reaction between borohydride and O_2, which results in the continuous formation of H_2, was confirmed by DEMS measurements performed in borohydride containing electrolyte under purely chemical conditions, in the absence of a Pt electrocatalyst, which also show considerable H_2 evolution. Depending on the potential, H_2 can also be generated by electrocatalytic oxidation of borohydride on the (Mg-free) Pt electrode, and possibly consumed by electrocatalytic H_2 oxidation. These reactions can proceed without a measurable Faradaic current when coupled to a simultaneous reduction reaction on the same electrode ('mixed potential' formation). Finally, in Mg^{2+} containing electrolyte, the ORR via reaction (9) can result in OH^-, which leads to the generation of insoluble $Mg(OH)_2$ products that appear as flakes in the borohydride containing electrolyte.

Discussion

Combining the results presented and discussed in the previous sections and previously reported data we arrive at the following main insights:

1. The initial efficiency for Mg deposition (in the first scan) in the O_2-free electrolytes is significantly enhanced in the presence of both additives, BH_4^- ($Mg(BH_4)_2$) and the crown ether 18-c-6, as compared to electrolyte I with only 18-c-6 as additive (see Figure S1 and Table 2). The same is true also for the reversibility in the first cycle. The fact that both additives are required for improved deposition/dissolution indicates a synergistic behavior with different roles of both additives, where borohydride acts as water scavenger and 18-c-6 as complexing agent, hindering the reductive decomposition of $TFSI^-$ in Mg-TFSI complexes. Sustained reversibility (also in subsequent cycles), however, is achieved only in electrolytes III and IV, which compared to electrolyte II contain double the amount of Mg^{2+}, as well as identical amounts of BH_4^- and 18-c-6 (in electrolyte III) or an excess of 18-c-6 (in electrolyte IV). Apparently, the Mg^{2+} concentration is important as well, which may reflect a decreasing sensitivity towards trace impurities with increasing Mg^{2+} concentration. Compared to previous findings for Mg deposition from the same electrolytes, but 50 times faster scan rate, the deactivation of reversible Mg deposition/stripping (per cycle) is much faster, reflecting the more efficient decomposition of the electrolyte due to the much longer interaction times.[15]

2. In electrolytes III and IV with their higher Mg^{2+} concentration DEMS results reveal an enhanced reductive decomposition of 18-c-6, as indicated by the potential dependent formation of ethene and methane (m/z = 15, 27, 28 fragments). This is proposed to happen upon reduction of its complex with Mg^{2+} ions. Possible deposits formed during this process such as (oligo–)polyethers on the electrode surface, however, do not (fully) inhibit reversible Mg deposition/stripping. Instead, the sustainable reversibility is enhanced.

3. The morphology of the electrodeposits formed during cycling strongly depends on the electrolyte composition. It changes from few individual particles in electrolyte I (Mg-$(TFSI)_2$ + 18-c-6) to overlapping hemispheres in electrolyte II ($Mg(BH_4)_2$ + 18-c-6) electrolyte, while in the electrolytes III and IV, with their twofold higher Mg concentration and different concentrations of 18-c-6 irregular structures (0.1 M 18-c-6, electrolyte III) and agglomerated particles (1 M 18-c-6, electrolyte IV) are formed. The latter particles exhibit also an additional internal structure. EDS analyses performed after cycling in the different O_2-free Mg-containing electrolytes are consistent with the conclusions derived from the DEMS measurements, with significant deposition of Mg and Mg (hydr–)oxy-species only in the presence of both additives. Signals of F, S, and N indicate the presence of TFSI decomposition products on the surface, but can also be due to traces of electrolyte remaining on the electrode after emersion. The same is true for borates, which could result from borohydride oxidation or from borohydrides in electrolyte traces on the surface that were oxidized after emersion. The concentrations of Mg and O obtained for electrolyte I are in the same range as those reported for Mg deposition from O_2-saturated BMP-TFFI-based electrolyte.[14]

4. Based on DEMS measurements performed in these different Mg-containing, but O_2-free electrolytes we could clearly identify an electrocatalytic oxidation of borohydride to borates, by reaction with H_2O trace impurities, which is indicated by a potential dependent H_2 evolution in the first cycle. The electrochemical borohydride oxidation seems to be significantly faster than the well-known bulk reaction between borohydride and water, as concluded from the much lower H_2 evolution in this electrolyte in the absence of the Pt electrode (Figure 3a). The measured H_2 evolution signal may furthermore be affected by H_2 electro-oxidation on the Pt electrode.

5. Borohydride oxidation/H_2 evolution is significantly enhanced upon O_2-saturation of the electrolyte, which is first of all due to a much faster chemical bulk reaction, as evidenced by the pronounced increase of H_2 formation upon the admission of O_2 in a purely chemical DEMS experiment without Pt electrode (Figure 3a). In the presence of Pt also the electro-catalytic borohydride oxidation via reactions (3) and (4) contribute, as supported by the distinct changes in the OCP upon admission of O_2 (see Figure 3b–3d). For current neutrality the current generated by these electrochemical reactions must be compensated by reduction reactions such as the ORR that proceed with similar current at the open circuit potential established upon admission of O_2 (mixed potential formation).

6. The reductive and oxidative Faradaic currents detected in CV measurements in O_2-saturated, Mg-containing electrolyte are at least partly due to the ORR and OER, as identified by the consumption and release of O_2 in online DEMS measurements in these electrolytes. This underlines the reversibility of the ORR/OER by deposition and re-oxidation of Mg peroxo-species, as the formation of MgO would inhibit this. Passivation of the Pt electrode is lower if both borohydride

ChemElectroChem

Research Article
doi.org/10.1002/celc.202300090

Chemistry Europe
European Chemical
Societies Publishing

and 18-c-6 are present, reflecting a reversible deposition/oxidation of Mg oxy-species. Furthermore, we could demonstrate that the reaction in borohydride containing solution results in a complex combination of different partial reactions between O_2, borohydride, 18-c-6 and water trace impurities, and also H_2 electro-oxidation, which occur depending on the potential and can be identified by comparison of Faradaic current, O_2 consumption/generation, water consumption/formation and H_2 formation. In addition, in O_2-saturated borohydride containing solutions also bulk chemical oxidation plays an important role, for example, by the formation of H_2. This is true at least in the initial phase of the reaction, before the depletion of borohydride in the electrolyte. Finally, different from O_2-free electrolytes, decomposition of 18-c-6 does not seem to play an important role in O_2-saturated electrolyte, as concluded from the absence of potential dependent decomposition signals such as $m/z = 15$.

7. The data indicate that the reversible Mg deposition/stripping and the OER/ORR in neat and O_2-saturated BMP-TFSI based electrolytes, respectively, require not only the presence of a reducing water scavenger (BH_4^-) and of a complexing agent (18-c-6), but depend sensitively also on the relative concentrations of Mg^{2+} and the two additives. Furthermore, while in the absence of O_2 the interaction between Mg^{2+} and 18-c-6 will cause slow decomposition of the Mg^{2+}-[18-c-6] additive, most likely by destructive reduction, this is not observed in the presence of O_2. We suggest that in this case the non-destructive removal of Mg^{2+} is facilitated via the reversible formation and deposition of MgO_2.

Overall, these DEMS measurements provided detailed insights into the complex reaction network active during potential cycling in O_2-free/O_2-saturated, Mg- and borohydride-containing BMP-TFSI electrolyte, extending our previous knowledge from CV measurements on the O_2-free electrolytes[15] and from DEMS measurements using NBH as water scavenger.[14] Particularly relevant for technical application in Mg-air batteries are the results that there is a highly efficient electrochemical pathway for reaction of the water scavenger BH_4^- with water, which depending on the potential and state of the electrode leads to H_2 evolution or H^+ formation and can proceed also under OCP conditions. In O_2-saturated borohydride-containing electrolyte the bulk chemical reaction between borohydride and O_2 is strongly enhanced and results in the generation of insoluble products, which appear as flakes in the electrolyte. This essentially excludes the use of BH_4^- as water scavenger in these electrolytes in Mg-air batteries.

Summary

As part of an extensive series of model studies on mechanistic aspects of the reactions in magnesium-air batteries we have performed systematic DEMS measurements on i) the deposition/stripping of Mg on a Pt film electrode in four different BMP-TFSI based electrolytes, containing $Mg(TFSI)_2$ and/or Mg-

$(BH_4)_2$ as Mg source, BH_4^- as water scavenger, and the crown ether 18-c-6 as complexing additive, and on ii) the reduction/evolution of O_2 in the same Mg-containing electrolytes. From the potential dependent appearance of different gaseous reaction products and electrolyte decomposition products and their correlation with the Faradaic current, we could identify a number of different reactions that occur in the above processes during potential cycling. These include deposition/stripping of Mg in O_2-free electrolyte and of Mg oxy-species in O_2-saturated electrolyte (ORR/OER), reductive (Mg-assisted) 18-c-6 decomposition, electrochemical borohydride oxidation by reaction with water traces, which at certain potentials is much more active than the well-known bulk chemical reaction, and the bulk chemical reaction between borohydride and O_2 or H_2O. Reaction with O_2 occurs at considerable rates in O_2-saturated electrolytes, which precludes the use of this water scavenger in Mg-air batteries. Overall, this work underlines the potential of DEMS measurements for a detailed understanding also of complex battery chemistries.

Experimental Section

The online DEMS experiments were performed in a beaker-type small-volume (about 0.5 cm³) DEMS cell, using a Pt film electrode sputtered onto a gas permeable membrane, which on the backside was directly interfaced to the vacuum chamber with the quadrupole mass spectrometer. A detailed description of the employed DEMS instrument was provided in that Ref. [62]. In short, the cell consists of a polyether ether ketone (PEEK) cylinder and a PEEK U-cup, which connects to the analysis chamber with the mass spectrometer (Pfeiffer Vacuum QMA 410) via a fluorinated ethylene propylene (FEP) membrane (Bola, purchased from Bolender, thickness 50 μm, exposed area 0.25 cm²). The cell was located in an Ar-filled glove box (MBraun LabMaster Pro, O_2 < 0.1 ppm; H_2O < 0.5 ppm) equipped with an O_2 supply line (Alphagaz, 99.9995 %), and connected to the external analysis chamber via a stainless steel bellow. For dismounting the cell, the connection to the analysis chamber could be closed with an open/close valve in the glove box. The Pt film working electrode (thickness ca. 70 nm) was sputtered onto the FEP membrane, using an Ar plasma sputter coater (Leica EM ACE600). Working electrodes of 13 mm diameter were punched from the Pt-sputtered membrane and stored in another Ar-filled glove box (MBraun LabStar, O_2 < 0.5 ppm; H_2O < 1 ppm). Before use they were dried in the glove box on a hot plate at 100 °C for ca. 30 min. Two fresh cuts from a Mg foil (99.9 %, Goodfellow, 0.25 mm thick), which were scratch-cleaned in a glove box environment, were used as counter and quasi-reference (−1.0 V vs. Fc/Fc$^+$) electrodes, respectively. In contrast to a Ag/AgCl reference, the Mg/MgO reference was found to be stable in these electrolytes also in the presence of O_2.[12,14] All potentials in this paper are given relative to that of the Mg/MgO reference. The DEMS cell was stored, assembled and operated in the glove box. For the electrochemical measurements we used a computer-controlled potentiostat (PAR 263 A), and the selected ion currents were acquired simultaneously. The mass spectrometric signals presented below are background corrected, such that the lowest value was set to zero.

Scanning Electron Microscopy (SEM) and Energy Dispersive Spectroscopy (EDS) characterization of the deposits was performed in a Zeiss Crossbeam 340 field-emission electron microscope, after extensive rinsing with acetone followed by drying under vacuum.

ChemElectroChem

Research Article
doi.org/10.1002/celc.202300090

Chemistry
Europe
European Chemical
Societies Publishing

The electrolytes were prepared in the glove box, by dissolving the appropriate amounts of $Mg(BH_4)_2$ (Sigma Aldrich, 95.0%), $Mg(TFSI)_2$ (Solvionic, 99.5%, <250 ppm H_2O) and 18-crown-6 ether (Alfa Aesar, 99.0%, <0.29% H_2O) in 1-butyl-1-methylpyrrolidinium bis(trifluoromethylsulfonyl) imide (BMP-TFSI, Solvionic, 99.9%, <20 ppm H_2O) under stirring (composition see Table 1). Karl Fischer titration of the resulting electrolytes yielded water contents in the range of ca. 30 ppm.[15] 0.5 mL of the respective electrolyte was filled into the DEMS cell, counter and reference electrode were introduced from the top. Together with the working electrode they were connected to the potentiostat to rest at the open circuit potential (OCP) until stable values of the OCP were obtained and the background signals of the corresponding ion currents had stabilized. For O_2 saturation the electrolytes were purged with O_2 by bubbling O_2 via a capillary immersed from the top, while the O_2-sensor of the MBraun LabMaster Pro glove box was deactivated. After each experiment with O_2 purging the glove box was flushed for 30 min to 1 h with Ar to reduce the O_2 content to <0.1 ppm.

Supporting Information

Acknowledgements

Conflict of Interests

The authors declare no conflict of interest.

Data Availability Statement

The data that support the findings of this study are available from the corresponding author upon reasonable request.

Keywords: Electrochemistry · Mg-air batteries · Mg electrodeposition/stripping · O_2 reduction/evolution · reaction mechanism

[1] L. J. Hardwick, C. Ponce de Leon, *Johnson Matthey Technol. Rev.* **2018**, *62*, 134–149.
[2] N. N. Rajput, T. J. Seguin, B. M. Wood, X. Qu, K. A. Persson, *Top. Curr. Chem. (Z)* **2018**, *376*, 19–46.
[3] Y.-T. Lu, A. R. Neale, C.-C. Hu, L. J. Hardwick, *Front. Energy Res.* **2021**, *8*, 602918.
[4] J. Drews, T. Danner, P. Jankowski, T. Vegge, J. M. Garcîa Lastra, R. Liu, Z. Zhao-Karger, M. Fichtner, A. Latz, *ChemSusChem* **2020**, *13*, 3599–3604.
[5] H. D. Yoo, I. Shterenberg, Y. Gofer, G. Gershinsky, N. Pour, D. Aurbach, *Energy Environ. Sci.* **2013**, *6*, 2265–2279.
[6] S. Tepavcevic, Y. Liu, D. Zhou, B. Lai, J. Maser, X. Zuo, H. Chan, P. Král, C. S. Johnson, V. Stamenkovic, N. M. Markovic, T. Rajh, *ACS Nano* **2015**, *9*, 8194–8205.
[7] D. Aurbach, Z. Lu, A. Schechter, Y. Gofer, H. Gizbar, R. Turgeman, Y. Cohen, M. Moshkovich, E. Levi, *Nature* **2000**, *407*, 724–727.
[8] J. Muldoon, C. B. Bucur, T. Gregory, *Angew. Chem. Int. Ed.* **2017**, *56*, 12064–12084; *Angew. Chem.* **2017**, *129*, 12232–12253.
[9] Z. Zhao-Karger, M. E. G. Bardaji, O. Fuhr, M. Fichtner, *J. Mater. Chem. A* **2017**, *5*, 10815–10820.
[10] Y. T. Law, J. Schnaidt, S. Brimaud, R. J. Behm, *J. Power Sources* **2016**, *333*, 173–183.
[11] M. Bozorgchenani, P. Fischer, J. Schnaidt, T. Diemant, R. M. Schwarz, M. Marinaro, M. Wachtler, L. Jörissen, R. J. Behm, *ChemElectroChem* **2018**, *5*, 2600–2611.
[12] Z. Jusys, J. Schnaidt, R. J. Behm, *J. Chem. Phys.* **2019**, *150*, 041724.
[13] D. Alwast, J. Schnaidt, K. Hancock, G. Yetis, R. J. Behm, *ChemElectroChem* **2019**, *6*, 1–12.
[14] M. Eckardt, D. Alwast, J. Schnaidt, R. J. Behm, *ChemSusChem* **2020**, *13*, 3919–3927.
[15] I. Weber, J. Ingenmey, J. Schnaidt, B. Kirchner, R. J. Behm, *ChemElectroChem* **2021**, *8*, 390–402.
[16] G. Vardar, A. E. S. Sleightholme, J. Naruse, H. Hiramatsu, D. J. Siegel, C. W. Monroe, *ACS Appl. Mater. Interfaces* **2014**, *6*, 18033–18039.
[17] M. Kar, Z. Ma, L. M. Azofra, K. Chen, M. Forsyth, D. R. MacFarlane, *Chem. Commun.* **2016**, *52*, 4033–4036.
[18] K. Karuppasamy, J. Theerthagiri, D. Vikraman, C.-J. Yim, S. Hussain, R. Sharma, T. Maiyalagan, J. Qin, H.-S. Kim, *Polymer* **2020**, *12*, 918.
[19] P. G. Bruce, S. A. Freunberger, L. J. Hardwick, J. M. Tarascon, *Nat. Mater.* **2012**, *11*, 19–29.
[20] D. Bresser, E. Paillard, S. Passerini, *J. Electrochem. Sci. Technol.* **2014**, *5*, 37–44.
[21] M. Kar, T. J. Simons, M. Forsyth, D. R. MacFarlane, *Phys. Chem. Chem. Phys.* **2014**, *16*, 18658–18674.
[22] S. Das, J. Højberg, K. B. Knudsen, R. Younesi, P. Johansson, T. Norby, T. Vegge, *J. Phys. Chem. C* **2015**, *119*, 18084–18090.
[23] G. A. Giffin, *J. Mater. Chem. A* **2016**, *4*, 13378–13389.
[24] N. Mozhzhukhina, A. Y. Tesio, L. P. M. De Leo, E. J. Calvo, *J. Electrochem. Soc.* **2017**, *164*, A518–A523.
[25] N. N. Rajput, X. Qu, N. Sa, A. K. Burrell, K. A. Persson, *J. Am. Chem. Soc.* **2015**, *137*, 3411–3420.
[26] X. Qu, I. Zhang, N. N. Rajput, A. Jain, E. Maginn, K. A. Persson, *J. Phys. Chem. C* **2017**, *121*, 16126–16136.
[27] F. Sagane, K. Ogi, A. Konno, K. Kanamura, *J. Electrochem. Soc.* **2019**, *166*, A5054–A5058.
[28] G. Giffin, A. Moretti, S. Jeong, S. Passerini, *J. Phys. Chem. C* **2014**, *118*, 9966–9973.
[29] T. Watkins, D. A. Buttry, *J. Phys. Chem. B* **2015**, *119*, 7003–7014.
[30] D. R. MacFarlane, J. M. Pringle, P. C. Howlett, M. Forsyth, *Phys. Chem. Chem. Phys.* **2010**, *12*, 1659–1669.
[31] S. Su, Y. NuLi, N. Wang, D. Yusipu, J. Yang, J. L. Wang, *J. Electrochem. Soc.* **2016**, *163*, D682–D688.
[32] Z. Ma, M. Kar, C. Xiao, M. Forsyth, D. R. MacFarlane, *Electrochem. Commun.* **2017**, *78*, 29–32.
[33] T. Watkins, A. Kumar, D. A. Buttry, *J. Am. Chem. Soc.* **2016**, *138*, 641–650.
[34] Y. Shao, T. Liu, G. Li, M. Gu, Z. Nie, M. Engelhard, J. Xiao, D. Lv, C. Wang, J. G. Zhang, *Sci. Rep.* **2013**, *3*, 3130.
[35] H. Wang, X. Feng, Y. Chen, Y.-S. Liu, K. S. Han, M. Zhou, M. H. Engelhard, V. Murugesan, R. S. Assary, T. L. Liu, W. Henderson, Z. Nie, M. Gu, J. Xiao, Ch. Wang, K. Persson, D. Mei, J.-G. Zhang, K. T. Mueller, J. Guo, K. Zavadil, Y. Shao, J. Liu, *ACS Energy Lett.* **2020**, *5*, 200–206.
[36] X. Gao, A. Mariani, S. Jeong, X. Liu, X. Dou, M. Ding, A. Moretti, S. Passerini, *J. Power Sources* **2019**, *423*, 52–59.
[37] P. Sabatier, *Ber. Dtsch. Chem. Ges.* **1911**, *44*, 1984–2001.
[38] P. Sabatier, *Ind. Eng. Chem.* **1926**, *18*, 1005–1008.

ChemElectroChem

Research Article
doi.org/10.1002/celc.202300090

**Chemistry
Europe**
European Chemical
Societies Publishing

[39] T. V. Sagar, J. Zavasnik, M. Finsgar, N. Novak Tusar, A. Pintar, *Catalysts* **2022**, *12*, 218–218_25.

[40] L. D. Chen, J. K. Norskov, A. C. Luntz, *J. Phys. Chem. C* **2015**, *119*, 19660–19667.

[41] J. G. Connell, B. Genorio, P. P. Lopes, D. Strmcnik, V. R. Stamenkovic, N. M. Markovic, *Chem. Mater.* **2016**, *28*, 8268–8277.

[42] J. G. Smith, J. Naruse, H. Hiramatsu, D. J. Siegel, *Chem. Mater.* **2016**, *28*, 1390–1401.

[43] Z. T. Xia, S. H. Chan, *J. Power Sources* **2005**, *152*, 46–49.

[44] D. S. Silvester, L. Aldous, C. Hardacre, R. G. Compton, *J. Phys. Chem. B* **2007**, *111*, 5000–5007.

[45] D. S. Silvester, K. R. Ward, L. Aldous, C. Hardacre, R. G. Compton, *J. Electroanal. Chem.* **2008**, *618*, 53–60.

[46] Y. Tang, L. Lin, A. Kumar, M. Guo, M. Sevilla, X. Zeng, *J. Phys. Chem. C* **2017**, *121*, 5161–5167.

[47] Z. Jusys, R. J. Behm, *Electrochem. Commun.* **2015**, *60*, 9–12.

[48] N. Dubouis, A. Serva, E. Salager, M. Deschamps, M. Salanne, A. Grimaud, *J. Phys. Chem. Lett.* **2018**, *9*, 6683–6688.

[49] J. Han, M. Zarrabeitia, A. Mariani, Z. Jusys, M. Hekmatfar, H. Zhang, D. Geiger, U. Kaiser, R. J. Behm, A. Varzi, S. Passerini, *Nano Energy* **2020**, *77*, 105176.

[50] J. Han, A. Mariani, M. Zarrabeitia, Z. Jusys, R. J. Behm, A. Varzi, S. Passerini, *Small* **2022**, *18*, 2201563.

[51] P. J. Linstrom, W. G. Mallard, "Mass Spectra" in NIST Chemistry WebBook; National Institute of Standards and Technology: Gaithersburg, MD 20899, **2010**.

[52] P. Hegemann, M. Hegemann, L. Zan, H. Baltruschat, *J. Electrochem. Soc.* **2019**, *166*, A245–A250.

[53] F. Gámez, P. Hurtado, B. Martínez-Haya, G. Berden, J. Oomens, *Int. J. Mass Spectr.* **2011**, *308*, 217–224.

[54] Z. Li, T. Diemant, Z. Meng, Y. Xiu, A. Reupert, L. Wang, M. Fichtner, Z. Zhao-Karger, *ACS Appl. Mater. Interfaces* **2021**, *13*, 33123–33132.

[55] M. Matsui, *J. Power Sources* **2011**, *196*, 7048–7055.

[56] Z. Ma, M. Forsyth, D. R. MacFarlane, M. Kar, *Green Energy & Environ.* **2019**, *4*, 146–153.

[57] Ch. Ling, D. Banerjee, M. Matsui, *Electrochim. Acta* **2012**, *76*, 270–274.

[58] M. Chatenet, F. Micoud, I. Roche, E. Chainet, J. Vondrák, *Electrochim. Acta* **2006**, *51*, 5452–5458.

[59] J. Schnaidt, T. N. Nguyen, Z. Jusys, R. J. Behm, *Electrochim. Acta* **2019**, *299*, 372–377.

[60] G. Vardar, E. G. Nelson, J. G. Smith, J. Naruse, H. Hiramatsu, B. M. Bartlett, A. E. S. Sleightholme, D. J. Siegel, C. W. Monroe, *Chem. Mater.* **2015**, *27*, 7564–7568.

[61] P. Reinsberg, C. Bondue, H. Baltruschat, *Electrochim. Acta* **2016**, *200*, 214–221.

[62] Z. Jusys, M. Binder, J. Schnaidt, R. J. Behm, *Electrochim. Acta* **2019**, *314*, 188–201.